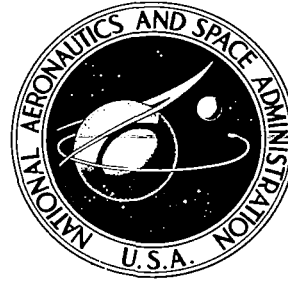


**NASA CONTRACTOR
REPORT**

NASA CR-1889



NASA CR-1889

C.1

0060997



TECH LIBRARY KAFB, NM

**LOAN COPY: RETURN TO
LOAN COPY: RETURN TO
AFWL (DOGL) M.
KIRTLAND AFB, N. M.**

**STATISTICAL PROPERTIES OF TURBULENCE
AT THE KENNEDY SPACE CENTER FOR
AEROSPACE VEHICLE DESIGN**

*by J. A. Dutton, H. A. Panofsky, D. C. Deaven,
B. R. Kerman, and V. Mirabella*

Prepared by
PENNSYLVANIA STATE UNIVERSITY
University Park, Pa.
for George C. Marshall Space Flight Center

NATIONAL AERONAUTICS AND SPACE ADMINISTRATION • WASHINGTON, D. C. • AUGUST 1971



0060997

TECHNICAL REPORT ST. FILE PAGE

1. REPORT NO. NASA CR-1889	2. GOVERNMENT ACCESSION NO.	3. RECIPIENT'S CATALOG NO.	
4. TITLE AND SUBTITLE STATISTICAL PROPERTIES OF TURBULENCE AT THE KENNEDY SPACE CENTER FOR AEROSPACE VEHICLE DESIGN		5. REPORT DATE August 1971	6. PERFORMING ORGANIZATION CODE
		8. PERFORMING ORGANIZATION REPORT #	
7. AUTHOR(S) J. A. Dutton, H. A. Panofsky, D. C. Deaven, B. R. Kerman, and V. Mirabella		10. WORK UNIT NO. 126-61-10-00-62	11. CONTRACT OR GRANT NO. NAS 8-21140
9. PERFORMING ORGANIZATION NAME AND ADDRESS Pennsylvania State University University Park, Pennsylvania		13. TYPE OF REPORT & PERIOD COVERED CONTRACTOR	
		14. SPONSORING AGENCY CODE	
12. SPONSORING AGENCY NAME AND ADDRESS NASA Washington, D. C. 20546			
15. SUPPLEMENTARY NOTES			
16. ABSTRACT The statistical properties of turbulence at the Kennedy Space Center as related to the design of aerospace vehicles are discussed, along with four major topics of boundary layer flows, namely, (1) the simulation of atmospheric turbulence with empirical orthogonal functions, (2) the estimation of co- and quad-spectra, (3) the estimation of viscous dissipation, and (4) estimation of the variances of turbulence.			
17. KEY WORDS Turbulence, viscous dissipation, orthogonal functions, velocity variance, coherence, self-similarity		18. DISTRIBUTION STATEMENT Unclassified - Unlimited	
19. SECURITY CLASSIF. (of this report) Unclassified	20. SECURITY CLASSIF. (of this page) Unclassified	21. NO. OF PAGES 68	22. PRICE \$3.00

TABLE OF CONTENTS

	Page
I. SIMULATION OF ATMOSPHERIC TURBULENCE WITH EMPIRICAL ORTHOGONAL FUNCTIONS	1
1.1 Introduction	1
1.2 Review of the method of decomposition	2
1.3 Computational methods	4
1.4 Characteristics of the eigenfunctions	6
1.5 Construction of simulated gust histories	9
References	16
II. ESTIMATION OF COHERENCE AND SLOPE	20
2.1 Introduction	20
2.2 Coherence	20
2.3 Slopes	29
2.4 Conclusion	38
References	38
III. THE ESTIMATION OF TOTAL DISSIPATION	40
3.1 Formulation of estimate	40
3.2 Results	41
References	46
IV. ESTIMATION OF VARIANCES	47
4.1 Variances at 18 meters	47
4.2 Change of variances with height	57
References	61

LIST OF FIGURES

Figure		Page
1.1	Normalized eigenfunctions computed from NAE data. The eigenvalues associated with each function are shown on the right. The plot spans 980 m of horizontal distance	7
1.2	Spectra of the normalized eigenfunctions shown in Figure 1.1 .	8
1.3	Sketch illustrating the algorithm used to obtain values of the coefficients by sampling from their distribution	11
1.4	Simulated turbulence records obtained as explained in the text (Equation 1.21) by combining the mean function and the gust function constructed with the sampled coefficients. The plot spans 980 m of horizontal distance	14
1.5	Statistical characterization of the simulated turbulence. The plotted numbers (1-9) represent the values found for the nine simulated time histories. The abscissa are standardized variables u_i/σ_{u_i} ($i = 1, 2, \dots, 9$). The solid line represents the Gaussian case. In the upper right, the dashed line represents the case of independence between the variable and its derivative. On the lower right, the coordinate is $\ln[N(u_i)/N(0)]$ and the abscissa is $(u_i/\sigma_{u_i})^2$	15
2.1	Decay constant of coherence of lateral wind component for the vertical separations between 18 m and 30 m as a function of the Richardson number at 23 m	26
2.2	Decay constant of coherence of the longitudinal component for the vertical separation between 18 m and 30 m as a function of the Richardson number at 23 m	27
2.3	Slope of lateral wind component between 18 m and 30 m as a function of the Richardson number at 23 m	33
2.4	Slope of the longitudinal wind component between 18 m and 30 m as a function of the Richardson number at 23 m	34
2.5	Decay constants of coherence for longitudinal and lateral wind components between 18 m and 30 m as a function of the normalized wind shear	36
2.6	Slope of the longitudinal and lateral wind components between 18 m and 30 m as a function of the normalized wind shear . . .	37

LIST OF FIGURES (continued)

Figure		Page
3.1	Ratio of the measured total dissipation above 18 m to the measured total dissipation below 18 m as a function of the gradient Richardson number.	44
3.2	Comparison of the measured (E_a) and estimated (E_T) vertically integrated dissipation in watts/m ² at and below 18 m	45
4.1	Variance of the longitudinal wind components at 18 m as function of friction velocity at 18 m utilizing a roughness length determined for each run separately	49
4.2	Variance of the lateral wind components at 18 m as a function of friction velocity at 18 m utilizing a roughness length determined for each run separately	50
4.3	Ratio of the variance of longitudinal wind components to friction velocity at 18 m as a function of the Richardson number at 18 m utilizing a roughness length determined for each run separately	51
4.4	Ratio of the variance of lateral wind components to friction velocity at 18 m as a function of the Richardson number at 18 m utilizing a roughness length determined for each run separately	52
4.5	Variance of the longitudinal wind components at 18 m as a function of friction velocity at 18 m utilizing a roughness length determined from averaged upwind zone conditions	53
4.6	Variance of the lateral wind components at 18 m as a function of friction velocity at 18 m utilizing a roughness length determined from averaged upwind zone conditions	54
4.7	Ratio of the variance of longitudinal wind components to the friction velocity at 18 m as a function of the Richardson number at 18 m utilizing a roughness length determined from averaged upwind zone conditions	55
4.8	Ratio of the variance of the lateral wind components to the friction velocity at 18 m as a function of the Richardson number at 18 m utilizing a roughness length determined from averaged upwind zone conditions	56
4.9	Difference of the variances of the longitudinal wind component at 18 m and 150 m as a function of the mean wind at 18 m	59
4.10	Difference of the variances of the lateral wind component at 18 m and 150 m as a function of the mean wind at 18 m	60

LIST OF TABLES

Table		Page
2.1	Decay constants for a_3^1 and a_3^2 for each run for selected levels	22
2.2	Decay factors in near-neutral air ($-0.2 \leq Ri \leq 0.2$)	28
2.3	Slopes S_3^1 and S_3^2 for each run for selected levels	30
2.4	Slope in near-neutral air ($-0.1 \leq Ri \leq 0.1$)	35
3.1	Vertically integrated dissipation of theoretical and observed methods for various runs	42

Section I

PREFACE

In the portion of the report which follows, we present the results of studies of the statistical structure of turbulence. Such studies performed under this contract have three aims:

- (1) To gather empirical evidence on the probabilistic aspects of turbulence in order to provide motivation and insight for development of theoretical models;
- (2) To compare the statistical structure of boundary layer turbulence at Cape Kennedy with that measured in other observational programs;
- (3) To attempt to use the resulting information in the construction of methods that can be used to take account of the effects of turbulence in the study and design of aerospace vehicles.

I. SIMULATION OF ATMOSPHERIC TURBULENCE WITH EMPIRICAL ORTHOGONAL FUNCTIONS

John A. Dutton and Dennis G. Deaven

1.1 Introduction

Simulated time histories of turbulent motion are required in a variety of engineering applications, and their use appears to be increasing as more sophisticated design studies are attempted. As one example, such time histories are used to provide a simulated environment for vehicle simulators used in the study of crew response to turbulence. As another, the time histories are necessary if non-linear effects are to be studied by analog or digital computation.

Several requirements must be imposed on time histories in such simulation studies if the effects of turbulence are to be determined accurately and in a useful manner. These include:

- (1) It must be possible to assess the likelihood of occurrence of any time history used in the simulation so that the degree to which results are representative is known.
- (2) The individual time histories must have the sequential characteristics of actual turbulence, the most notable being that the energy spectrum should be proportional to the $-5/3$ power of the wave-number or frequency over quite a wide range.
- (3) The time histories should exhibit the probabilistic structure of actual turbulence, modeling correctly the observed non-Gaussian behavior of the density function and the exceedance statistics.

A consequence of the last two requirements is that the simulated turbulence will contain the element of surprise so prevalent in actual turbulence.

Most methods for simulating turbulence now in use fail to satisfy all three criteria (Dutton, 1968). The use of observed records will obviously satisfy the last two requirements but it appears difficult to satisfy the first. We present here an initial study of a method that offers considerable potential. It is based on the Loeve (1963) decomposition of turbulent time histories using the empirical orthogonal functions discussed by Dutton (1969) in NASA CR-1410.

1.2 Review of the Method of Decomposition

The empirical orthogonal functions are obtained from an ensemble $\{u(t)\}$ of time histories of turbulence by forming the covariance matrix

$$(1.1) \quad R(t, t') = E \{u(t) u(t')\}$$

and solving the integral equation defined on an appropriate domain

$$(1.2) \quad \int R(t, t') \phi_n(t') dt' = \lambda_n \phi_n(t)$$

for the eigenvalues, λ_n , and the eigenfunctions, ϕ_n . The eigenfunctions satisfy the orthonormality condition

$$(1.3) \quad \int \phi_n(t) \phi_m(t) dt = \delta_{mn}$$

and we have an expansion for each function, $u(t)$, in the form

$$(1.4) \quad u(t) = \sum_{n=1}^{\infty} a_n \phi_n(t)$$

in which

$$(1.5) \quad a_n = \int u(t) \phi_n(t) dt$$

The coefficients are also orthogonal across the ensemble in the sense that

$$(1.6) \quad E \{a_n a_m\} = \lambda_n \delta_{nm}$$

and thus it can be shown that

$$(1.7) \quad R(t, t') = \sum_{n=1}^{\infty} \lambda_n \phi_n(t) \phi_n(t')$$

The significant fact about the eigenfunctions is that if we arrange them in order of decreasing λ_n , then for each N , the expansion

$$(1.8) \quad u_N(t) = \sum_{n=1}^N a_n \phi_n(t)$$

will explain more of the variance in the ensemble than would be explained by any other set of functions in the sense that the error

$$(1.9) \quad e_N = E \{u(t) - u_N(t)\}^2$$

is a minimum.

Thus the empirical orthogonal functions provide a scheme in which the characteristics of temporal sequencing common to the ensemble are represented

by the eigenfunctions, and the individual variations for each time history are represented in the coefficients.

The simulation method to be studied here involves the following steps:

- (1) Obtain a large ensemble of time histories of turbulence;
- (2) Find the eigenfunctions, eigenvalues, and the coefficients of each of the time histories;
- (3) Determine the probabilistic structure of the coefficients;
- (4) Obtain simulated time histories with known likelihood of occurrence (with respect to the original ensemble) by sampling from the distribution of the coefficients.

This scheme should meet all three criteria stated in the introduction; this is a report on a first attempt to carry out the program represented by the four steps above to determine whether there is indeed a possibility of success.

1.3 Computational Methods

At the time the previous report (Dutton, 1969) was prepared, we were not able to find eigenfunctions for time histories because of computational restrictions on the length of the data sample.

In practice, we have N time histories, each with M points. The correlation function is approximated by (we now use averages across the finite ensemble to replace the expectation, E)

$$(1.10) \quad R(t_i, t_j) = \frac{1}{N} \sum_{n=1}^N u_n(t_i) u_n(t_j)$$

and this is a matrix of size $M \times M$. If we let D be the $N \times M$ matrix containing the observed data, then the correlation matrix is $R = D^T D / N$ and this is of

order $M \times M$. When the time histories contain several hundred points it becomes uneconomical to find the eigenvalues and eigenvectors for R by matrix diagonalization.

An alternative approach has been suggested by Hirose and Kutzbach (1969). We form instead the matrix

$$(1.11) \quad S = D D^T / N$$

which is of order $N \times N$, and thus, in our case with turbulence, very much smaller than R . Now we let L_S and V_S be the (diagonal) eigenvalue and the eigenvector matrices associated with S . Then, because we can have at most N positive eigenvalues, $L_S = L_R$. The transformation

$$(1.12) \quad V_R = D^T V_S (L_S N)^{-1/2}$$

gives the eigenvectors for R . (For a proof see, Law and Fariss, 1968.) Thus the diagonalization necessary to find the eigenvectors is performed on a smaller matrix, S , and then V_R is obtained by matrix multiplication.

In this study, we use three gust time histories obtained by the National Aeronautical Establishment of Canada (Mather, 1967); statistical characteristics of these records have been discussed by Dutton (1968) and Dutton, Thompson, and Deaven (1969). Some 1024 points from each component for each of three runs were selected to give nine time histories. The 1024 points represent a total distance of 980 m; the sampling interval was 9.5 m. The ensemble of nine histories was normalized so that

$$(1.13) \quad E \{u(t_j)\} = \frac{1}{9} \sum_{n=1}^9 u_n(t_j) = 0 \quad (j = 1, 2, \dots, M)$$

and so that

$$(1.14) \quad E \left\{ \frac{1}{T} \int_0^T u^2 dt \right\} = \frac{1}{9} \sum_{n=1}^9 \left\{ \frac{1}{1024} \sum_{j=1}^{1024} u_n^2(t_j) \right\} = 1$$

Thus there were eight non-zero eigenvalues and eigenfunctions possible representing the eight linearly independent normalized time histories.

1.4 Characteristics of the Eigenfunctions

The resulting eigenfunctions appear, as might be expected, to be similar to time histories of turbulence themselves. The function associated with the largest eigenvalue explained 66 percent of the variance in this ensemble. The eigenfunctions are shown in Figure 1.1. Two points are worth noting in the figure. The high-frequency content appears to increase with the order of the eigenvalue. Moreover, abrupt changes presumably associated with surprise occur in the higher order eigenfunctions; note particularly those in the fourth, fifth, and seventh eigenfunctions.

The variance spectra of the eigenfunctions were computed to determine whether the second criterion would be satisfied. The spectra shown in Figure 1.2 reveal the $-5/3$ slope over most the range of wave-numbers present, with some loss of low-frequency energy in the spectra of the higher order functions.

The expansion defined by Equation 1.4 shows that the Fourier transforms will obey the relation

$$(1.15) \quad \hat{u}_T(\omega) = \frac{1}{\sqrt{2\pi T}} \int_0^T u(t) e^{-i\omega t} dt = \sum_{n=1}^N a_n \hat{\phi}_{n_T}(\omega)$$

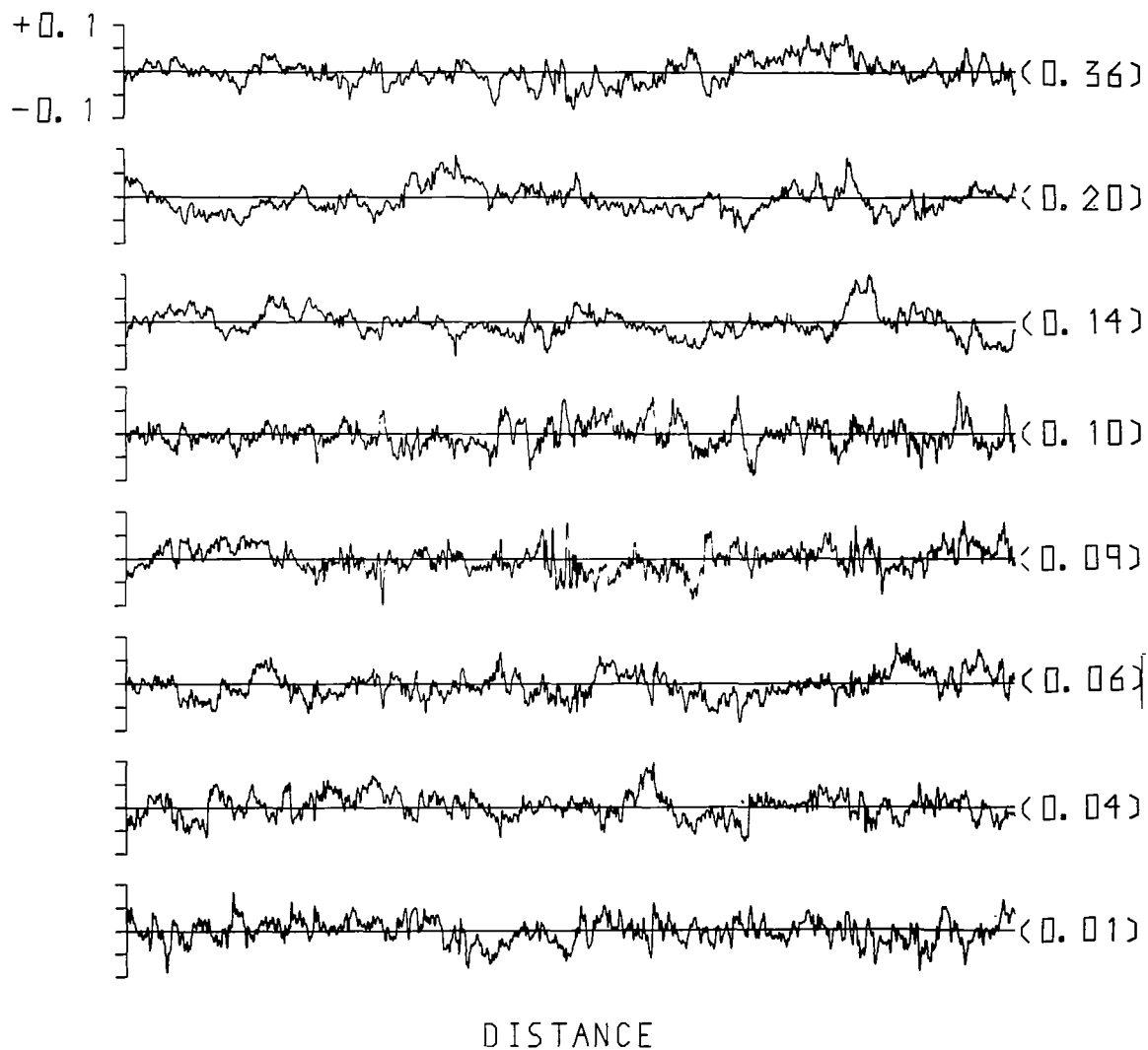


Figure 1.1 Normalized eigenfunctions computed from NAE data. The eigenvalues associated with each function are shown on the right. The plot spans 980 m of horizontal distance.

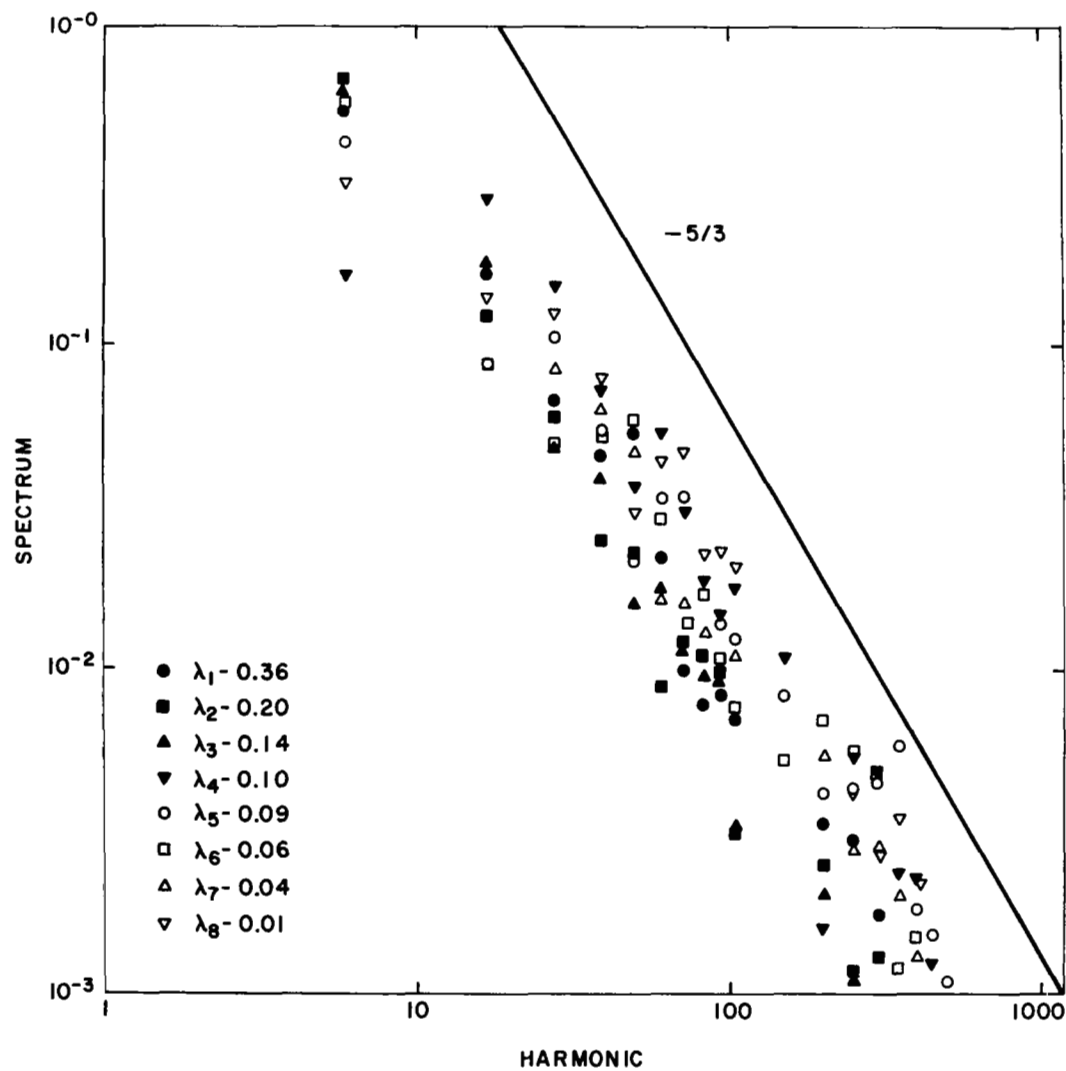


Figure 1.2 Spectra of the normalized eigenfunctions shown in Figure 1.1.

and thus, taking account of Equation 1.6, the average spectrum becomes

$$(1.16) \quad \Phi(\omega) = E \{ |\hat{u}_T(\omega)|^2 \} = \sum_{n=1}^N \lambda_n |\hat{\phi}_{n_T}(\omega)|^2 = \sum_{n=1}^N \lambda_n \Phi_n(\omega)$$

where Φ_n is the spectrum of the n^{th} eigenfunction. Thus the average spectrum will have the required $-5/3$ behavior.

1.5 Construction of Simulated Gust Histories

The simulation method being studied here, proposed by Dutton (1968), uses these eigenfunctions to construct artificial time histories simulating turbulence. Suppose that in addition the lack of correlation expressed by Equation 1.4, the coefficients were also independent in the sense that the probability density function obeys a relation

$$(1.17) \quad p(a_1, a_2, \dots, a_n) = p_1(a_1) p_2(a_2) \dots p_n(a_n)$$

Then we could form the distribution function,

$$(1.18) \quad F_i(a) = \int_{-\infty}^a p_i(\xi) d\xi, \quad (i = 1, \dots, N)$$

in which the subscript denotes the function associated with the coefficients of i^{th} order, and then use a random number generator to produce variates from a Gaussian population. Let r be such a number and let the Gaussian distribution function be $F_G(r)$. Then a coefficient, a , with a cumulative probability $F_G(r)$ is obtained from the operation

$$(1.19) \quad a(r) = F_i^{-1} [F_G(r)]$$

which F_i^{-1} is the function inverse to F_i , that is

$$(1.20) \quad F_i^{-1} [F_i(a)] = a$$

A sketch of the computational procedure is shown in Figure 1.3. Clearly a sample of coefficients whose distribution approaches the observed one will be produced as increasingly large sample are obtained in this manner.

If we let $r = (r_1, r_2, \dots, r_N)$ be a vector of independent, Gaussian variables, and if Equation 1.17 holds, the probability of the particular realization

$$(1.21) \quad u_{\tilde{r}}(t_j) = \bar{u}(t_j) + \sum_{n=1}^N a(r_n) \phi_n(t_j) \quad (j = 1, \dots, M)$$

obtained from the simulated gust profiles about the ensemble mean $\bar{u}(t)$, can be assessed from the probability density

$$(1.22) \quad p = p_G(r_1) p_G(r_2) \dots p_G(r_N)$$

In the finite case represented by eigenvectors obtained from Equation 1.10 only N of the M values $u_{\tilde{r}}(t_j)$ are independent of each other because any N values in the second term of Equation 1.22 could be used to solve for N coefficients a_n . To see why this is true, note that the initial data records contain $N \times M$ pieces of information. The eigenfunctions are linear combinations of these data and represent $N \times M$ pieces of information subject to the orthonormality condition (Equation 1.3). Hence there are $N \times N$ pieces of

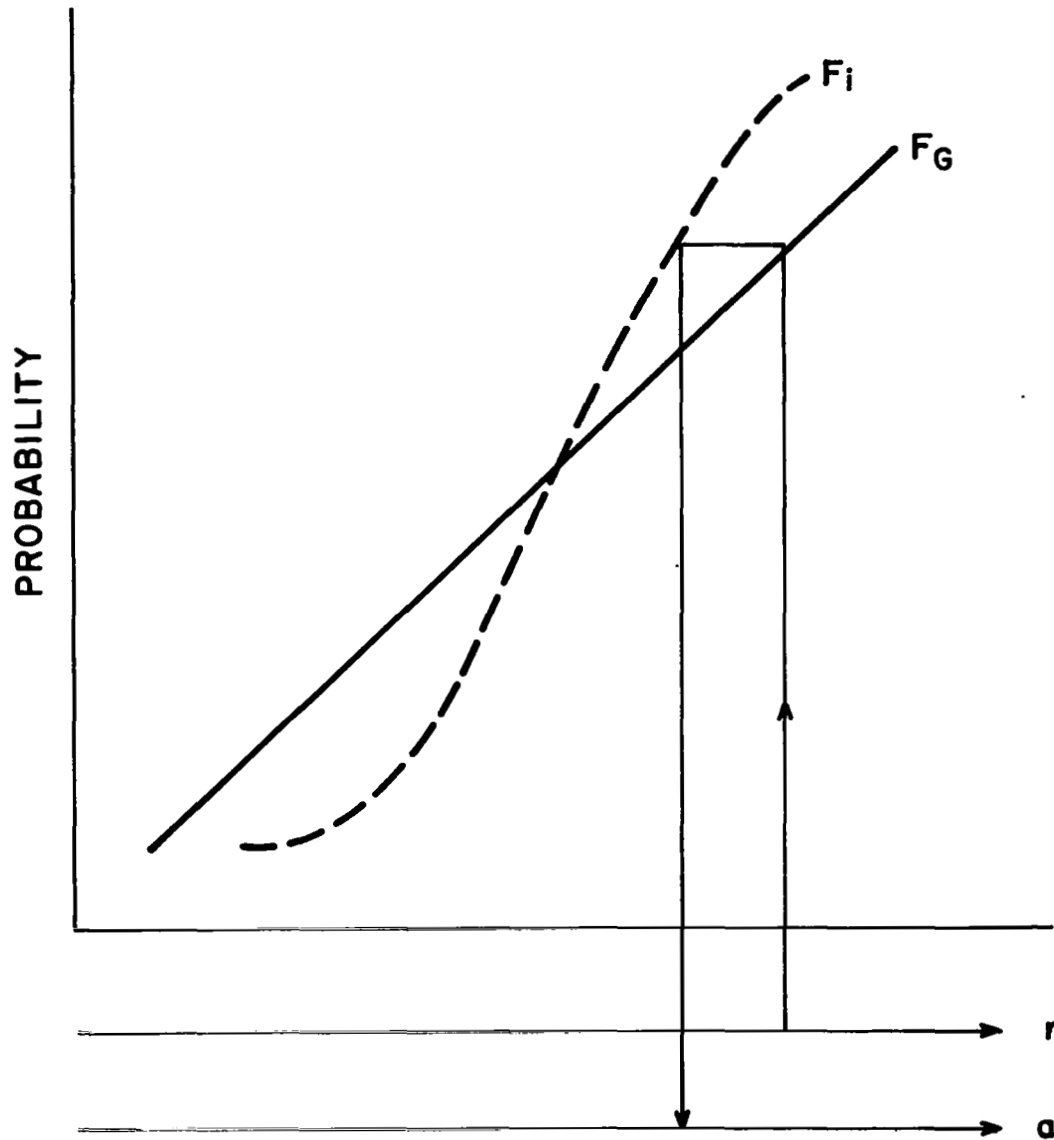


Figure 1.3 Sketch illustrating the algorithm used to obtain values of the coefficients by sampling from their distribution.

information in the eigenfunction set that are not independent and so the eigenfunctions contain $(N \times M) - (N \times N)$ independent pieces of information. The coefficients $\{a_n\}$ are another set of $(N \times N)$ pieces of information, and in combination with the eigenfunctions, will give back the original data set with $N \times M$ pieces of information. Of course Equation 1.6 shows that the coefficients only have $N \times (N - 1)$ independent pieces of information, the N final independent data being the eigenvalues themselves.

Thus we have a conditional probability problem. First, we must determine the probability of encountering the ensemble (or covariance matrix) with which we began. This probability can presumably be estimated by considering the ensemble in relation to the total collection of empirical data about turbulence. Next we must determine the probability of obtaining a particular function by sampling in this ensemble, a probability characterized by the N^{th} order joint distribution

$$(1.23) \quad P_u(u_1, u_2, \dots, u_N) = \int_{-\infty}^{u_1} \dots \int_{-\infty}^{u_N} P_u(\xi_1, \dots, \xi_N) d\xi_1 d\xi_N$$

in which $u_i = u(t_i)$.

With equation 1.21 we find that

$$(1.24) \quad P_u(u_1, \dots, u_N) du_1 \dots du_N = p(a_1, \dots, a_N) \left| \frac{\partial(u_1, \dots, u_N)}{\partial(a_1, \dots, a_N)} \right| da_1, \dots, da_N$$

But we have assumed that the coefficients are independent and that each depends on r , so that

$$(1.25) \quad p_u(\xi_1, \dots, \xi_N) d\xi_1, \dots, d\xi_N =$$

$$\prod_{i=1}^N p_G(r_i) \frac{da_i}{dr_i} \left| \frac{\partial(u_1, \dots, u_N)}{\partial(a_1, \dots, a_N)} \right| dr_1 \dots dr_N$$

The Jacobian determinant contains values of the eigenfunctions, $\phi_1(t_1)$, $\phi_1(t_2)$, \dots , $\phi_2(t_1)$, $\phi_2(t_2)$, \dots , $\phi_N(t_N)$

From Equation 1.25 we see that if da_i/dr_i is approximately constant or a maximum near $r_i = 0$, then the time histories with the largest probability within the ensemble will be those obtained when $r_1 = r_2 = \dots = r_N = 0$. Thus the most likely function obtained by sampling is the one for which $a_1 = a_2 = \dots = a_N = 0$, and so the most likely function $u_r(t)$ is the mean function $\bar{u}(t)$.

A sample of nine simulated time histories was obtained in this manner, assuming that Equation 1.17 is true. The simulated turbulence records are shown in Figure 1.4; their statistical characteristics illustrated in Figure 1.5.

The simulated time histories, as a group, have the correct behavior near the origin of the probability density function, but do not appear to contain as many very large gusts as the original data. The exceedance statistics shown in Figure 1.4 verify this conclusion.

The apparent failure to represent the large gusts correctly may very well be due to a dependence between the coefficients of the various functions in the ensemble. The next step in the investigation is to pursue the questions associated with this possible dependence.

The appearance of some degree of dependence would not seriously compromise the method; sampling would have to be done from joint distributions rather than individual ones. On the basis of the results presented here it appears

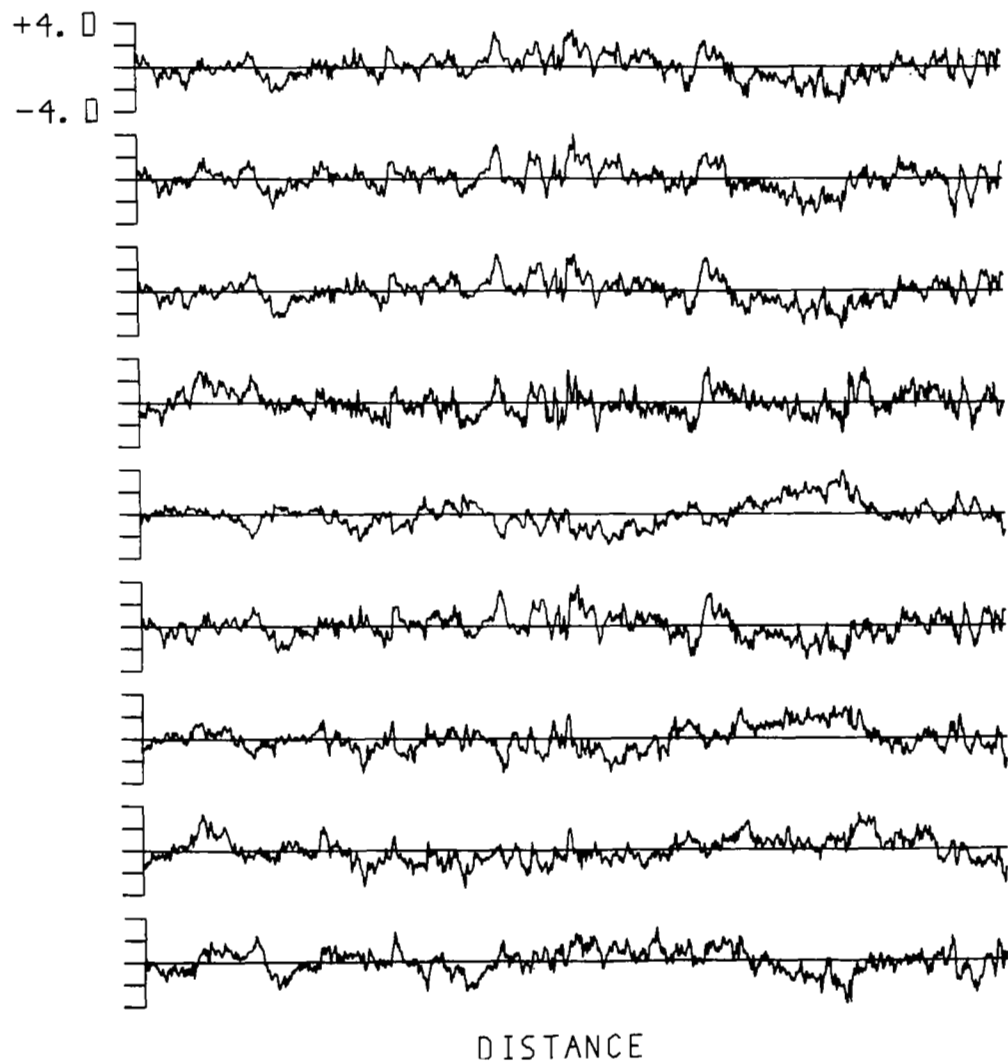


Figure 1.4 Simulated turbulence records obtained as explained in the text (Equation 1.21) by combining the mean function and the gust function constructed with the sampled coefficients. The plot spans 980 m of horizontal distance.

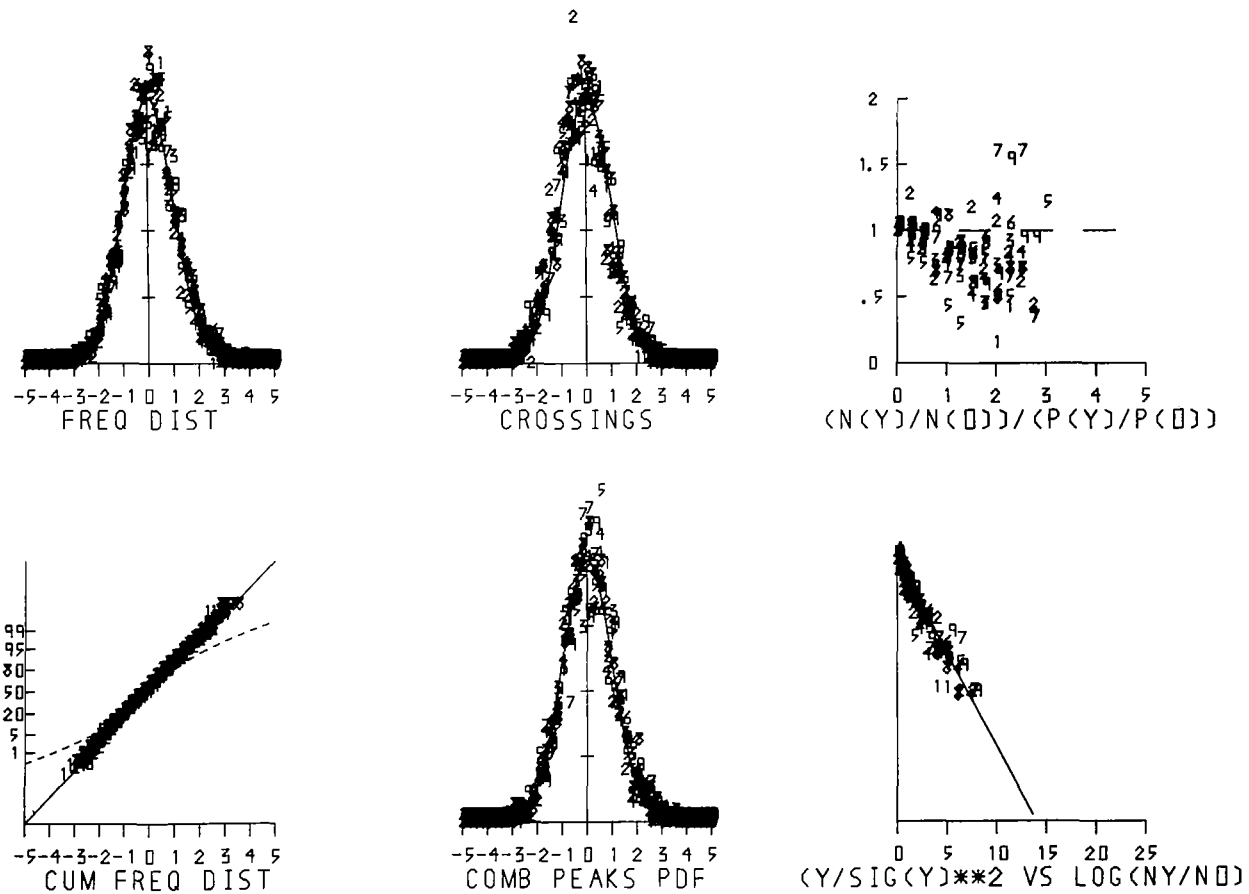


Figure 1.5 Statistical characterization of the simulated turbulence. The plotted numbers (1-9) represent the values found for the nine simulated time histories. The abscissa are standardized variables, u_i/σ_{u_i} ($i=1,2,\dots,9$). The solid line represents the Gaussian case. In the upper right, the dashed line represents the case of independence between the variable and its derivative. On the lower right, the coordinate is $\ln[N(u_i)/N(0)]$ and the abscissa is $(u_i/\sigma_{u_i})^2$.

that the method is a qualified success, and that further investigation and testing are merited.

REFERENCES

- Dutton, J. A., 1968: Broadening horizons in prediction of the effects of atmospheric turbulence on aeronautical systems, AIAA Paper 68-1065. To appear in *Progress in Aeronautical Sciences*, Pergamon Press.
- Dutton, J. A., 1969: A preliminary study of the probabilistic structure of turbulent forcing of launch vehicles. Investigation of the Turbulent Wind Field Below 150 M Altitude at the Eastern Test Range, NASA Contractor Report CR-1410.
- Dutton, J. A., G. J. Thompson, and D. G. Deaven, 1969: The probabilistic structure of clear air turbulence: some observational results and implications. Clear Air Turbulence and Its Detection, Y. H. Pao and A. Goldberg, eds., Plenum Press, New York.
- Hirose, M. and J. Kutzbach, 1969: An alternate method for eigenvector computations. J. Appl. Met., 8, 701.
- Law, V. J. and R. H. Fariss, 1968: On the relations between eigenvalues and eigenvectors for matrices resulting from pre- and post-multiplication by the transpose. Math Computation, 22, 867-868.
- Loéve, M., 1963: Probability Theory, D. Van Nostrand Co., Inc., Princeton, N. J.
- Mather, G. K., 1967: Some measurements of mountain waves and mountain wave turbulence made using the NAE T-33 turbulence research aircraft. National Aeronautical Establishment, National Research Council, Canada.

PREFACE
to

SECTIONS II, III, and IV

A considerable number of wind statistics at the Kennedy tower can be estimated from the roughness length (see chapter 3), and the winds and temperatures at 18 m and 30 m only.

First, the winds and temperature are used to define a Richardson number at 23 m, from which L follows by Businger's hypothesis:

$$L_o = 23 \text{ m/Ri}$$

Then the surface stress is given by

$$\sqrt{\frac{\tau_o}{\rho}} \equiv u_{*o} = \frac{kv_{18}}{\ln \frac{18\text{m}}{z_o} - \psi(z/L_o)}$$

Standard deviations of u at 18 m follow by multiplying u_{*o} by 2.3. The standard deviation of v is obtained by multiplications of u_{*o} by a quantity which can be read as function of z/L from Figure 4.4.

Standard deviations at other levels are obtained by subtracting from the standard deviations at 18 m quantities obtained as function of V_{18} from Figures 4.9 and 4.10.

Dissipation rates at various levels are given by:

$$\epsilon = \frac{u_{*o}^3}{k^2} \left[\left(1 - 18 \frac{z}{L_o} \right)^{-1/4} - \frac{z}{L_o} \right]$$

These can also be used to estimate high-frequency portions of the u and v spectra (up to about $1/k = 3z$) by applying

$$S(k) = a \epsilon^{2/3} k^{-5/3}$$

where a is about 0.50 for u and 0.65 for v , if k is in radians per unit length.

Coherences up to 100 m height are obtained from

$$\text{coh}(n) = e^{-a \frac{n\Delta z}{\bar{V}}}$$

where a is 19 for u and 13 for v . Δz is the height difference and \bar{V} is the mean wind in Δz , which is sufficiently accurately given (for this purpose) by

$$\bar{V} = v_{18} (\bar{z}/18)^{0.25}$$

Slopes are 2.0 for v and 1.0 for u below 100 m and 1.0 and 0.3 above 100 m.

Cospectra and quadrature spectra are prescribed by:

$$\text{cosp}(n) = \sqrt{S_1(n)S_2(n)\text{coh}(n)} \cos \frac{2\pi n\Delta z s}{\bar{V}}$$

and

$$\text{quad}(n) = \sqrt{S_1(n)S_2(n)\text{coh}(n)} \sin \frac{2\pi n\Delta z s}{\bar{V}}$$

In general, winds at high levels on the tower can be estimated from

$$V = v_{18} \left(\frac{z}{18\text{m}} \right)^\beta$$

where β depends on $\frac{z}{z_0}$ and $\frac{z}{L}$. The optimum relationship for Kennedy is now under study.

In order to obtain $Ri = z/L$ for some of the computations above, winds at two levels were needed. However, z/L can be estimated from a bulk Richardson number at 18 m:

$$B = g \frac{\gamma_d - \gamma}{T} \frac{z^2}{v_{18}^2}$$

according to nomograms prepared by Panofsky and Prasad (1965). The usefulness of this nomogram for Kennedy data is now being investigated, and empirical corrections may be applied. If successful, all the estimates discussed here can be made from wind observations at 18 m only.

In future work, the various statistics will be related to information available on weather charts and atlases.

REFERENCES

- Panofsky, H. A., and B. A. Prasad, 1965: Similarity theories and diffusion, Air and Water Pollution, 9, 419-430.

II. ESTIMATION OF COHERENCE AND SLOPE

H. A. Panofsky and B. R. Kerman

2.1 Introduction

A general system describing missile response to atmospheric forcing can be based on the covariance tensors of Cartesian velocity components. This tensor, for a scalar component for a time lag t , and positional separation Δx_i , can be written

$$R_i^j(t, \Delta x_i) = \int_0^\infty \bar{S}(n) \sqrt{\text{coh}_i^j(n)} \cos 2\pi n \left(\frac{\Delta x_i^j}{V} S_i^j - t \right) dn \quad (2.1)$$

where $\bar{S}(n)$ is geometric mean of the spectra of the component at two positions and S_i^j is the slope of the maximum correlation with distance Δx_i^j . The coherence, $\text{coh}_i^j(n)$, has been demonstrated to be well approximated by $\exp(-a_i^j \Delta f^i)$ (Davenport, 1961), where $\Delta f^i = \frac{n \Delta x_i^j}{V}$ which, if Taylor's hypothesis is satisfied, is the ratio of the displacement to the wavelength. It will be the purpose of this section to demonstrate some new estimates for parameters describing the coherence and slope of horizontal wind components, both under neutral stratification, and tentatively under stable and unstable stratification.

2.2 Coherence

As mentioned previously, the coherence has been shown to be well represented as

$$\text{coh}_j^i(\Delta f^j) = \exp(-a_j^i \Delta f^j) \quad (2.2)$$

where $\Delta f^j = \frac{n \Delta x^j}{V}$ and $i, j = 1, 2, 3$ refer to longitudinal, lateral and vertical

wind components. An excellent survey of collated results from numerous previous experiments as well as that at Cape Kennedy is given by Pielke (1969).

Considering for the moment only previous results of Cape Kennedy data, Pielke found that, under neutral stratification, the decay constant for longitudinal components for vertical separations $a_3^1 \sim 22$ and that for lateral components $a_3^2 \sim 18$. Pielke's results were based on a subjective best fit curve for estimates of the appropriate decay constant. Since previous computations by Shiotani (1969) and Davenport (1961) had arrived at estimates of $a_3^1 \sim 17$ and $a_3^2 \sim 13$ a more objective re-evaluation of a_3^1 and a_3^2 including additional data was undertaken.

Accordingly, a computerized analysis was devised to fit a negative exponential by non-linear least squares regression utilizing the Marquardt algorithm (Marquardt, 1963). Standard convergence criteria were used as supplied with the algorithm program. However the F and t-test criteria needed therein were relaxed from 10% to 25% due to the dispersion of coherence estimates as seen in sample computer plots. A range of Δf from 0 to .12 was selected so as to eliminate high frequency noise effects. Several difficulties arose with such an approach.

The first problem was a lack of convergence in about 10 to 15% of the computations due to bad data. The second difficulty arose from the varying data format between the 1967 and 1968 data. The latter instead of having 15 combinations of coherence between the levels 18, 30, 60, 90, 120 and 150 m has only the 3 combinations 18-30, 60-90 and 120-150 m. This made inclusion of the 1968 results with the 1967 results only possible on a level by level basis instead of a weighting according to low or high mean heights. The results are tabulated in Table 2.1.

TABLE 2.1
Decay Constants for a_3^1 and a_3^2 for Each Run for Selected Levels

Run	Ri_{23}	Longitudinal a_3^1			Lateral a_3^2		
		18-30	60-90	120-150	18-30	60-90	120-150
030	-0.16	21.4	22.6	22.4	13.7	15.0	13.5
067	-0.32	21.5	17.6	20.8	11.4	13.8	13.1
086	-0.28	16.8	35.1	32.4	11.0	18.0	27.2
091	-0.17	16.8	13.4	10.9	12.6	9.9	7.4
101	-0.23	13.6	12.9	11.2	8.7	8.3	6.5
121	-1.01	15.9	24.9	10.2	23.0	8.4	18.0
133	-0.14	17.0	18.2	14.0	13.5	15.0	12.2
138	-2.36	12.9			9.8		
139	-0.69	19.0	27.1	17.2		28.9	38.0
141	-2.32	19.5	30.2	19.0	10.2	28.4	16.5
142	0.08	21.6	23.8	34.5	14.0	33.4	
143	0.11	38.3	35.2	73.2	27.8	11.7	33.8
144	0.14	11.4	69.2	48.7		97.3	38.8
149	-0.60	25.1	18.1				
151	-9.75	13.6		40.1			
155	-0.31	11.8	13.8	12.8			
156	0.02	20.0		81.8		28.2	29.3
162	-0.20				14.3		16.6
163	-0.33	29.4	42.1	33.1	29.6	25.6	36.2
165	-0.21	23.2	19.8	20.4			
176	-1.08	18.3	14.0	14.8			
182	-0.46	12.1	21.6	13.2	9.0	13.4	10.1
183	-0.39	11.4	30.5	18.7	17.1	36.2	15.2
189	-0.85	24.9	33.8	25.3			
196	-0.44	24.2	26.1	23.2	16.4	17.5	15.8
299	-0.07	17.8	13.2	18.2	9.0	9.3	9.7
305	-0.09	22.9	18.4	16.1	12.8	17.0	11.8
308	-0.06	18.9	23.7		39.1	51.0	
319	-2.54	17.9	11.7	12.6	14.4	18.4	

TABLE 2.1 (continued)

Run	R_{23}	Longitudinal a_3^1			Lateral a_3^2		
		18-30	60-90	120-150	18-30	60-90	120-150
327	0.00				15.8		
351	-0.69	15.4	18.1	15.7	16.2	25.9	15.1
355	-0.59	17.3	18.0	11.6	11.9	21.4	17.8
359	-0.12	19.3	26.3	15.0	14.0	12.9	13.9
361	-0.09	16.1	34.9	13.6	14.5	9.9	11.7
364	-0.48	22.7	27.5	15.5	15.3	15.7	11.1
366	-0.50	15.9	21.3	12.6	9.6	14.5	9.2
367	-3.39	14.6	4.2	6.7	12.2	14.8	12.6
369	0.07	16.6	9.1	8.5	12.2	7.6	6.2
377	0.08				10.7		
380	0.01	15.1	19.4		11.1	10.5	
389	0.08	18.3	18.1	19.5	15.4	30.5	13.4
394	0.03	22.0	21.7		12.8	13.9	
415	0.00	20.3	16.1	12.6	12.7	11.3	6.1
447	0.05				13.9	17.1	10.1
477	-0.12				10.4		
478	0.00	14.5	20.7	18.3	14.0	17.2	10.4
480	0.00	15.3	12.0	27.7	12.5	11.0	11.7
481	0.04	18.1	18.8	31.4	13.7	17.5	9.8
515	-0.28	20.8	25.1	16.1	11.1	14.6	14.0
521	-0.07	19.4	20.3	20.3	12.1	14.7	22.1
526	-0.36	7.0	20.1	8.8	5.6	12.0	7.9
536	0.10	17.4	32.4	29.0	15.5	19.9	17.9
546	0.34	29.0	33.5		21.5	58.9	26.0
551	-8.50	8.3	9.8	13.6	15.5	15.9	7.0
555	-1.48	8.4	12.6	8.5	8.1	5.9	54.2
565	0.00	19.9		28.8	11.5	19.8	27.0
567	0.02	16.7	28.5	28.2	20.3	20.8	22.1
610	-1.36	18.1	14.6	9.9	12.0	10.4	6.2
614	0.07	20.4	21.4	11.9	25.6	17.1	12.6
618	-0.33	20.9	19.3	18.3	11.5	15.6	16.8
619		19.3	21.4	20.6	12.2	13.4	14.1

TABLE 2.1 (continued)

Run	Ri_{23}	Longitudinal a_3^1			Lateral a_3^2		
		18-30	60-90	120-150	18-30	60-90	120-150
625		7.6	5.2		21.8		3.9
627		21.8	27.9	17.2	16.8	19.7	15.4
631		23.9	12.7	10.8	31.1	13.3	12.7
633		18.1	16.8	31.6	18.9	9.8	9.7
641		12.2	17.3	12.3	19.6	27.6	10.9
648		13.9	21.1	11.0	11.3	7.5	15.6

After a cursory examination of the results no discernible relations could be found between the "a" values and height. Accordingly, to study the effect of stratification upon the a_j^i , it was decided to concentrate on the 18-30 level pair initially where the Richardson number was best determined.

Figure 2.1 shows the estimates arrived at by the least squares fit of the lateral wind component's coherence between the levels 18 and 30 m, plotted as a function of the Richardson number based on Chaplin's (Blackadar, et al., 1969) work. The upper curve represents Pielke's fit to the Cape Kennedy data; the lower curve, Pielke's fit of Shiotani's, Davenport's and other's results. The box represents the closure of the estimates in near-neutral ($-0.2 \leq Ri \leq 0.2$) fit whose weighted average (based on the number of coherence estimates for $0 \leq \Delta f \leq .12$, for each fit) is given by the solid straight line and whose weighted average standard deviation is denoted by the dashed straight lines. As can be seen the revised estimate of $a_3^2 = 13.22 \pm 1.18$ is in excellent agreement with results from other sites.

Figure 2.2 represents the analogous analysis for the longitudinal wind components. Again the upper solid curve represents Pielke's fit of Cape Kennedy data, the lower solid curve other workers' results. The decay constant $a_3^1 \sim 18.57 \pm 1.19$ arrived at by an identical averaging procedure as explained for the lateral component. Again the averaged neutral value is in excellent agreement with the fit of results from sites excluding Cape Kennedy.

A hypothesis was tested that the decay constant for the coherence representation were proportional to the Monin-Obukhov similarity variable

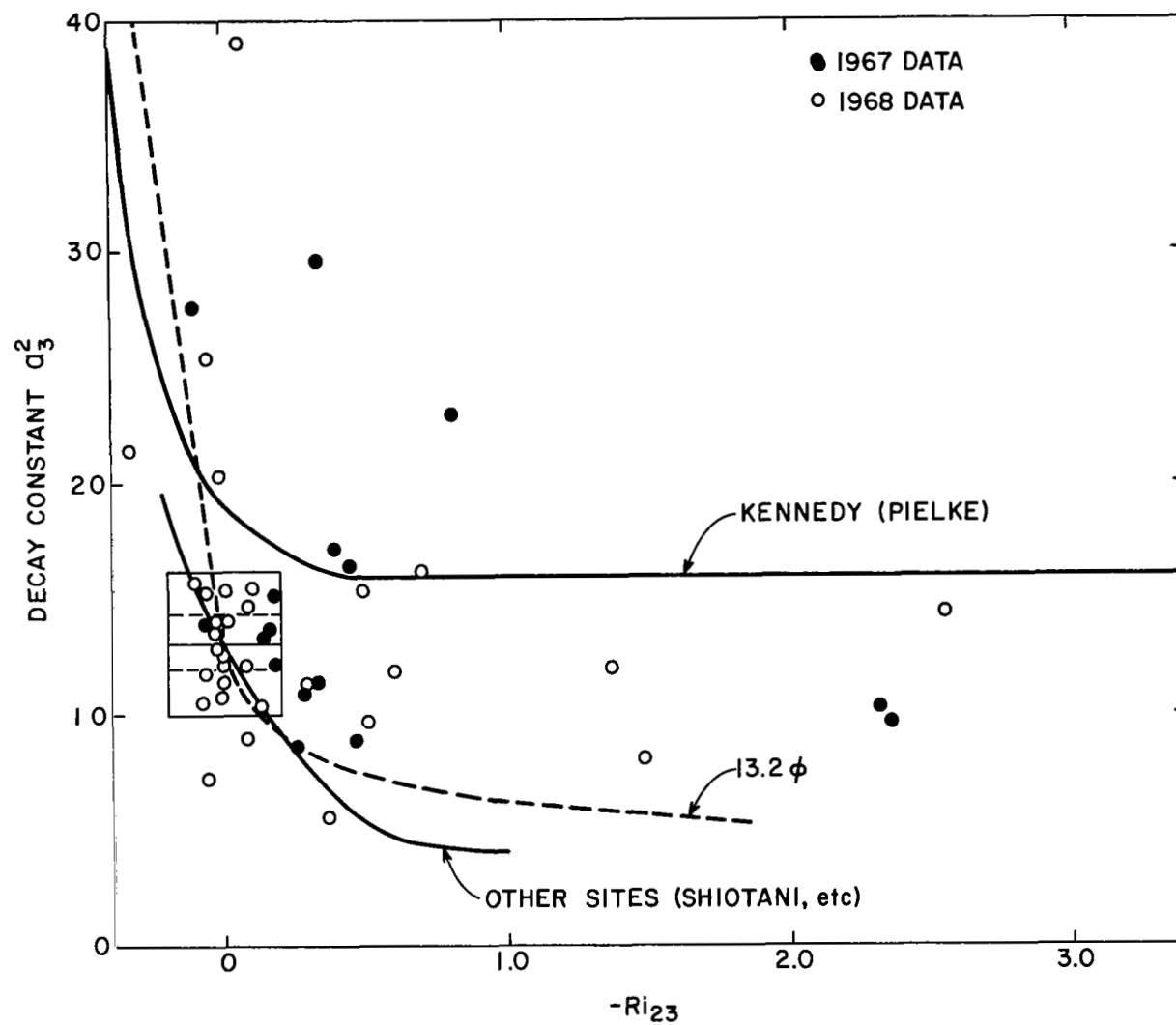


Figure 2.1 Decay constant of coherence of lateral wind component for the vertical separations between 18 m and 30 m as a function of the Richardson number at 23 m.

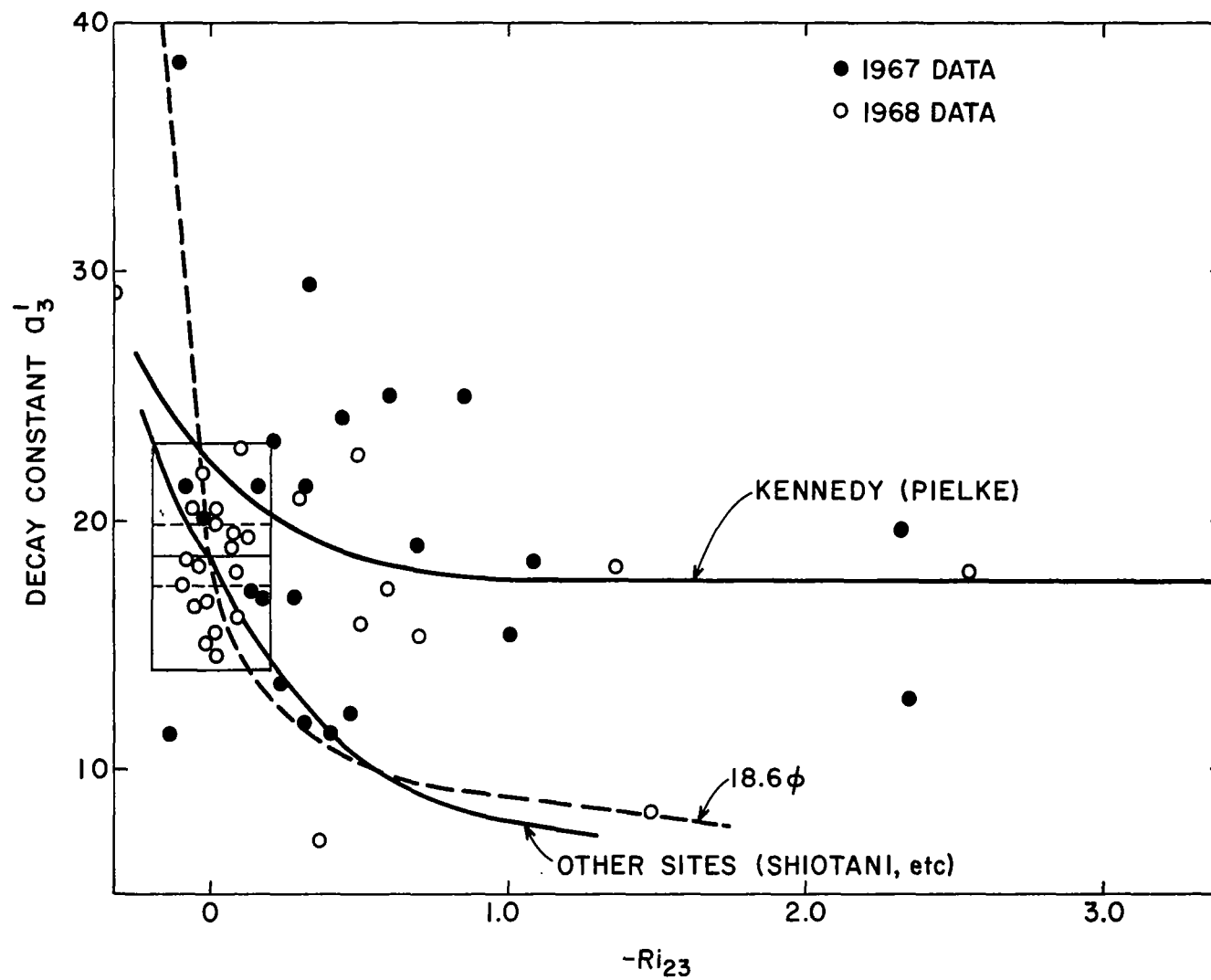


Figure 2.2 Decay constant of coherence of the longitudinal component for the vertical separation between 18 m and 30 m as a function of the Richardson number at 23 m.

(Monin, 1954) ϕ defined as

$$\phi = \frac{kz}{u_*} \frac{\partial \bar{u}}{\partial z} \quad (2.3)$$

the curves 13.22ϕ and 18.57ϕ , were plotted as functions of the 18-30 m Richardson number (Businger, 1966) in Figures 2.1 and 2.2 respectively. "a" values and ϕ 's appear to behave in similar ways. To test the Cape Kennedy data fit explicitly, Figure 2.5 is a plot of the lateral and longitudinal decay constants vs 13.22ϕ and 18.57ϕ respectively. As can be seen the fit is not good.

The averaging technique for near-neutral stratification was extended to the 60-90 m and 120-150 m level pairs based on a linear extrapolation of Richardson number with height based on the Pandolfo (1966) hypothesis. Table 2.2 tabulates the results.

Table 2.2

Decay factors in near-neutral air ($-0.2 \leq Ri \leq 0.2$)

Level	a_{lon} (neutral)	a_{lat} (neutral)
18-30	18.6	13.2
60-90	21.3	16.3
120-150	20.9	14.2

Within the errors of measurement, the near-neutral "a" values can be considered constant with height.

2.3 Slopes

The slope S_i^j introduced in Equation 2.1, can be defined as

$$S_i^j = \frac{1}{2\pi\Delta f^i} \tan^{-1} \frac{\text{quad}(\Delta f^i)}{\text{cosp}(\Delta f^i)} \quad (2.4)$$

where quad and cosp are the quadrature and cospectra respectively. Pielke in his thesis found that the vertical slopes for lateral and longitudinal wind components S_3^2 and S_3^1 were 2.6 and 1.0 respectively. To strengthen his conclusions further data from Cape Kennedy were analyzed.

S_i^j was fitted as a linear least squares approximation to the slope of the function $\tan^{-1} \frac{\text{quad}(\Delta f^i)}{\text{cosp}(\Delta f^i)}$ vs. $2\pi \Delta f^i S_i^j$ utilizing the normal regression equations, i.e.

$$\langle S_i^j \rangle = \frac{\sum_{m=1}^N \tan^{-1} \frac{\text{quad}_m(\Delta f^i)}{\text{cosp}_m(\Delta f^i)}}{2\pi \sum_{m=1}^N (\Delta f^i)_m} \quad (2.5)$$

where N is the total number of estimates of $0 \leq \Delta f^i \leq 0.12$. The averaging to evaluate $\langle S_i^j \rangle$ was carried out on a level to level basis as well as on a high-low, height distinction basis and an overall value for all heights for the 1967 data and on a level to level basis for the 1968 data. The results are tabulated in Table 2.3.

Figures 2.3 and 2.4 represent the results for the 18-30 m level combination graphically. The solid curve in each case represents Pielke's original fit on the basis of data from all possible sites. Box averaging, as employed with the decay constants, gave mean values under neutral stratification of $S_3^1 = 1.02$ and $S_3^2 = 1.99$. The value $S_3^1 = 1.02$ agrees with the previously established

TABLE 2.3
Slopes S_3^1 and S_3^2 for Each Run for Selected Levels

Run	Ri_{23}	Longitudinal			Lateral		
		18-30	60-90	120-150	18-30	60-90	120-150
030	-0.16	0.86	0.88	0.78	1.75	2.31	1.48
067	-0.32	0.43	0.12	0.17	0.98	1.09	0.58
086	-0.28	0.65	0.81	1.45	1.63	2.83	0.82
091	-0.17	0.29	0.64	0.18	1.31	0.94	0.95
101	-0.23	1.04	0.77	0.40	1.03	0.73	0.63
121	-1.01	1.01	0.62	0.11	0.96	0.38	0.94
133	-0.14	0.37	1.02	0.75	1.35	1.12	0.32
138	-2.36	0.78		0.39	0.96		0.15
139	-0.69	1.43	0.13	0.28	2.79	0.71	1.62
141	-2.32	0.56	1.04	0.27	1.13	1.09	1.36
142	0.08	1.12	1.27	0.45	1.87	2.02	1.61
143	0.11	1.05	0.64	1.00	2.35	1.34	0.21
144	0.14	0.50	0.39	1.15	2.44	0.19	2.44
149	-0.60	0.04	0.26	0.32			
151	-9.75	0.82	2.97	0.98			
155	-0.31	0.76	0.30	1.27			
156	0.02	1.18	1.94	1.96	2.74	1.93	0.47
162	-0.20				0.57	0.54	0.31
163	-0.33	0.21	0.33	0.22	1.50	1.57	0.56
165	-0.21	0.58	0.00	0.66			
176	-10.8	0.76	0.18	0.82			
182	-0.46	0.67	0.62	0.33	1.50	0.02	0.21
183	-0.39	0.40	0.73	0.30	1.70	1.64	0.16
189	-0.85	0.90	0.88	0.39			
196	-0.44	0.44	0.27	0.61	2.08	1.84	0.21
299	-0.07	0.64	0.52	0.28	1.54	1.05	0.84
305	-0.09	1.11	0.16	0.23	1.85	1.41	0.39
308	-0.06	0.95	0.73	0.04	2.37	4.74	1.83

TABLE 2.3 (continued)

Run	R1 ₂₃	Longitudinal			Lateral		
		18-30	60-90	120-150	18-30	60-90	120-150
319	-2.54	0.65	0.08	0.24	1.52	1.16	1.88
351	-0.69	0.05	0.25	0.31	1.41	1.92	1.08
355	-0.59	0.57	0.58	0.52	1.02	0.35	0.11
359	-0.12	0.49	0.55	0.18	1.85	1.32	0.84
361	-0.09	1.60	0.86	0.08	2.29	1.52	0.93
364	-0.48	0.13	0.04	0.03	1.47	1.26	1.21
366	-0.50	0.44	0.79	0.01	1.53	1.17	0.86
367	-3.39	0.34	0.81	1.36	0.28	0.63	1.24
369	0.07	0.92	0.84	0.01	1.53	1.28	0.18
380	0.01	0.74	0.25		1.81	1.59	
389	0.08	1.33	0.63	1.07	2.01	2.06	1.70
394	0.03	1.04	1.02		1.94	2.29	
415	0.00	0.62	0.73	0.32	2.09	1.73	1.12
447	0.05				1.24	2.03	1.07
477	-0.12	1.14	0.02	1.07	1.77	0.74	0.25
478	0.00	0.79	1.52	1.03	2.11	2.53	1.78
480	0.00	1.46	0.76	0.96	2.65	2.23	1.38
481	0.04	0.96	0.30	0.05	1.82	1.49	0.82
515	-0.28	0.45	0.02	0.24	1.32	1.34	0.86
521	-0.07	0.66	1.77	0.89	2.06	2.36	0.94
526	-0.36	0.43	0.38	1.14	1.94	1.30	0.37
536	0.10	1.83	2.56	0.47	2.25	2.75	0.03
546	0.34	1.60	0.58	0.34	1.57	3.39	2.79
551	-8.50	0.41	0.00	0.11	1.20	0.06	0.27
555	-1.48	0.64	0.49	0.24	1.62	0.59	0.61
565	0.00	1.39	0.63	0.97	1.99	1.99	0.92
567	0.02	0.21	1.95	1.34	2.50	2.97	1.08
610	-1.36	0.77	0.57	0.16	1.37	1.84	0.92
614	0.07	0.83	1.15	0.50	1.12	1.31	0.98
618	-0.33	0.18	0.80	0.43	1.60	1.56	1.10
619		1.40	1.70	0.80	1.69	1.35	0.69

TABLE 2.3 (continued)

Run	Ri_{23}	Longitudinal			Lateral		
		18-30	60-90	120-150	18-30	60-90	120-150
625		0.44	0.23	0.23	0.59	1.86	0.59
627		1.54	1.98	0.67	1.96	1.85	1.01
631		1.75	0.77	0.37	2.22	1.75	1.65
633		1.09	0.90	0.97	2.25	1.59	1.51
641		1.22	1.90	0.29	1.88	1.06	0.93
648		0.60	0.16	1.24	1.10	0.95	0.07

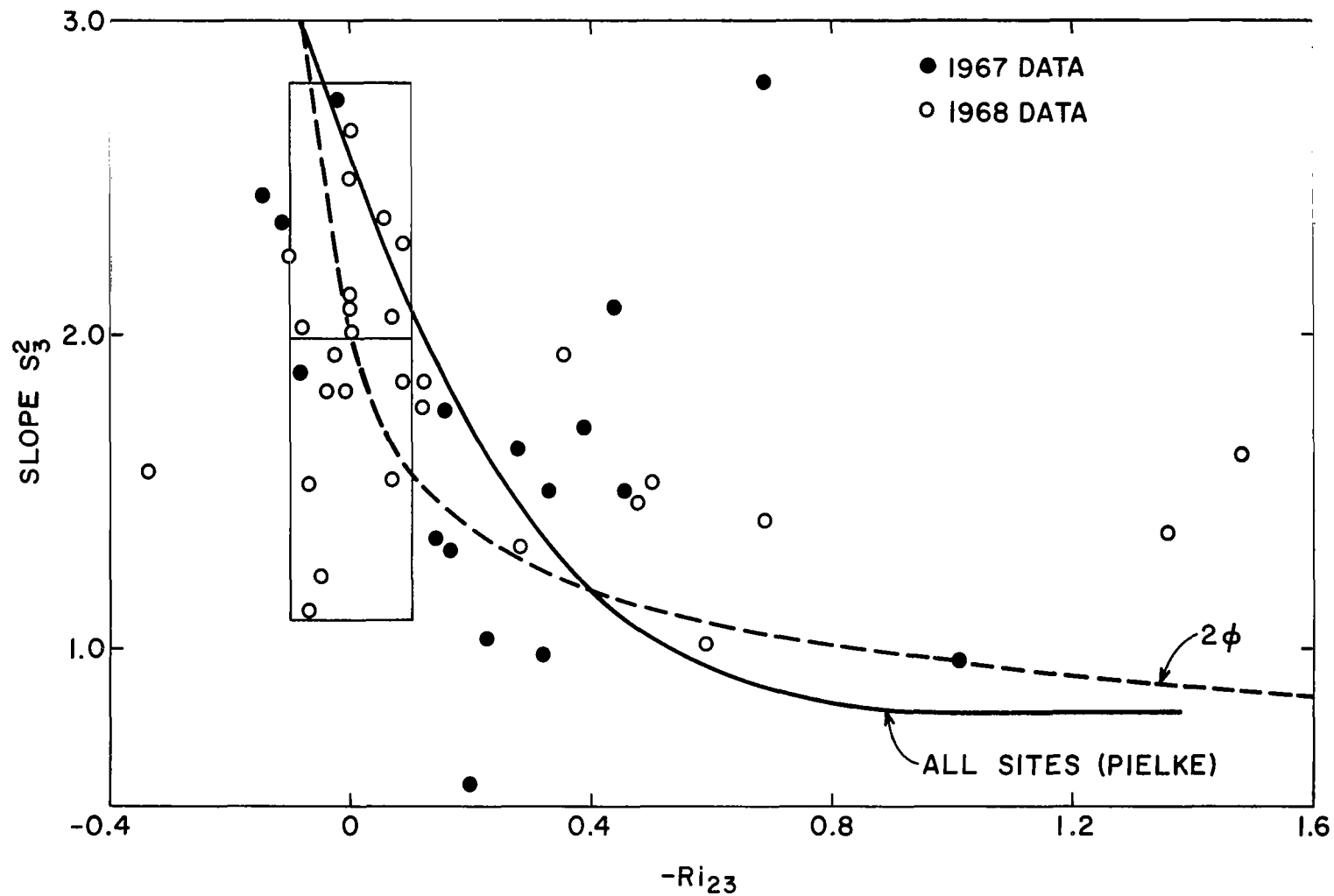


Figure 2.3 Slope of lateral wind component between 18 m and 30 m as a function of the Richardson number at 23 m.

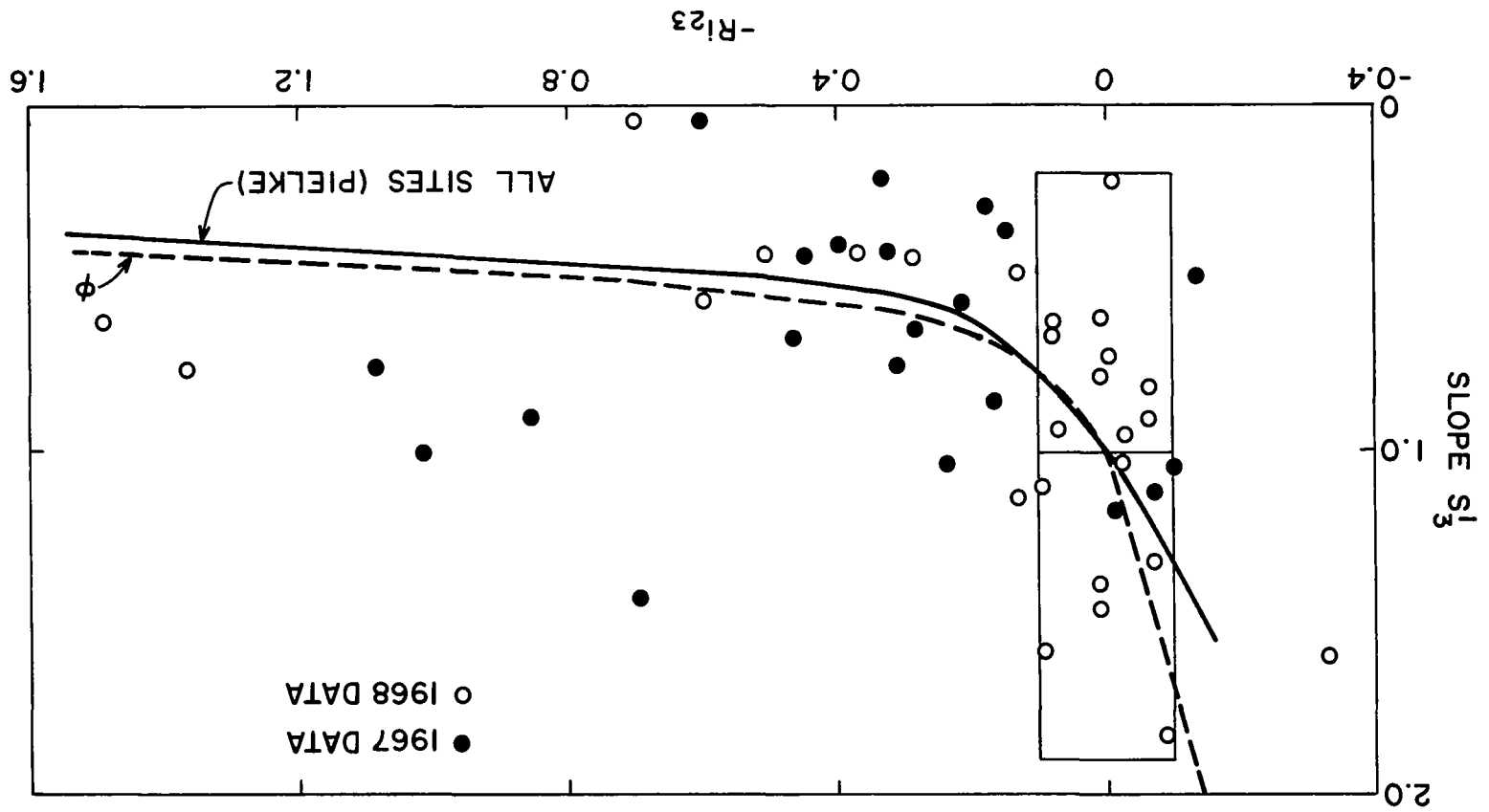


Figure 2.4 Slope of the longitudinal wind component between 18 m and 30 m as a function of the Richardson number at 23 m.

value of unity. However the value $S_3^2 \sim 2$, although speculated by Pielke, does not agree well with the results of all other studies.

Again, as a hypothesis, the slopes were considered to be proportional to the Monin-Obukhov similarity variable ϕ . Intuitively, slopes should be proportional to wind shear, and ϕ is a normalized wind shear. Accordingly values of 2ϕ and ϕ are plotted on Figures 2.3 and 2.4. The correspondence in each case is displayed graphically in Figure 2.6. The lateral slopes seem to be slightly underestimated while the longitudinal slopes fit well.

As with the decay constant 'a', the slopes for near neutral stratification were averaged. Here, the definition of near-neutral was revised to $-0.1 \leq Ri \leq 0.1$. The results for near neutral air are presented in Table 2.4.

TABLE 2.4

Slope in near-neutral air ($-0.1 \leq Ri \leq 0.1$)

Level	Slope _{lon} (neutral)	Slope _{lat} (neutral)
18-30	1.02	1.99
60-90	1.03	2.05
120-150	0.76	1.00

The slopes in near-neutral air appear to be constant up to about 100 m and show a major decrease above this height. Therefore the hypothesis that the slopes are proportional to the non-dimensional wind shear ϕ cannot be applied above about 100 m. This follows from Pandolfo's hypothesis that ϕ in neutral air would be unity at all levels but the results show the slopes decreasing. Accordingly the effects of decreasing stress and Ekman inertia must be included.

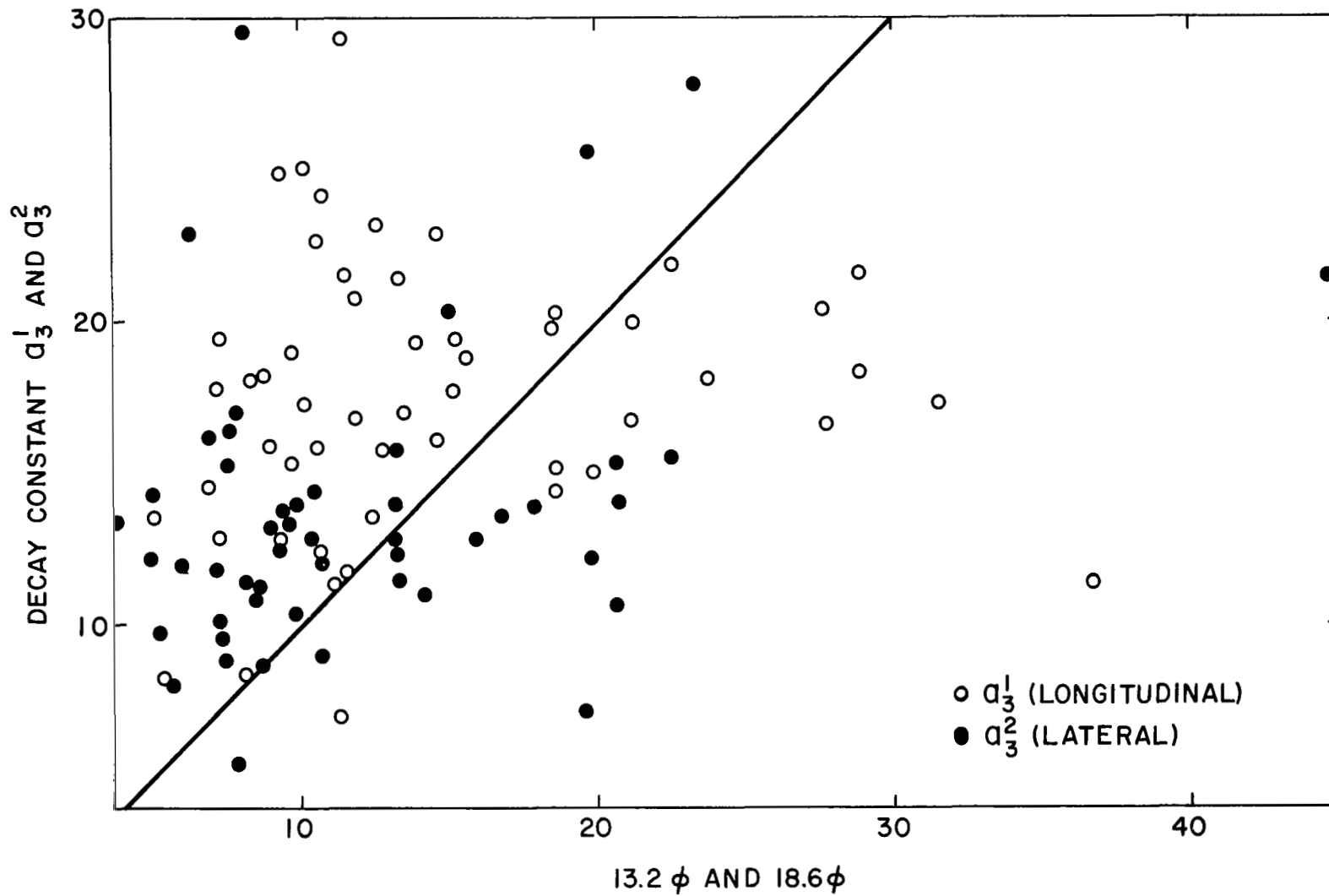


Figure 2.5 Decay constants of coherence for longitudinal and lateral wind components between 18 m and 30 m as function of the normalized wind shear.

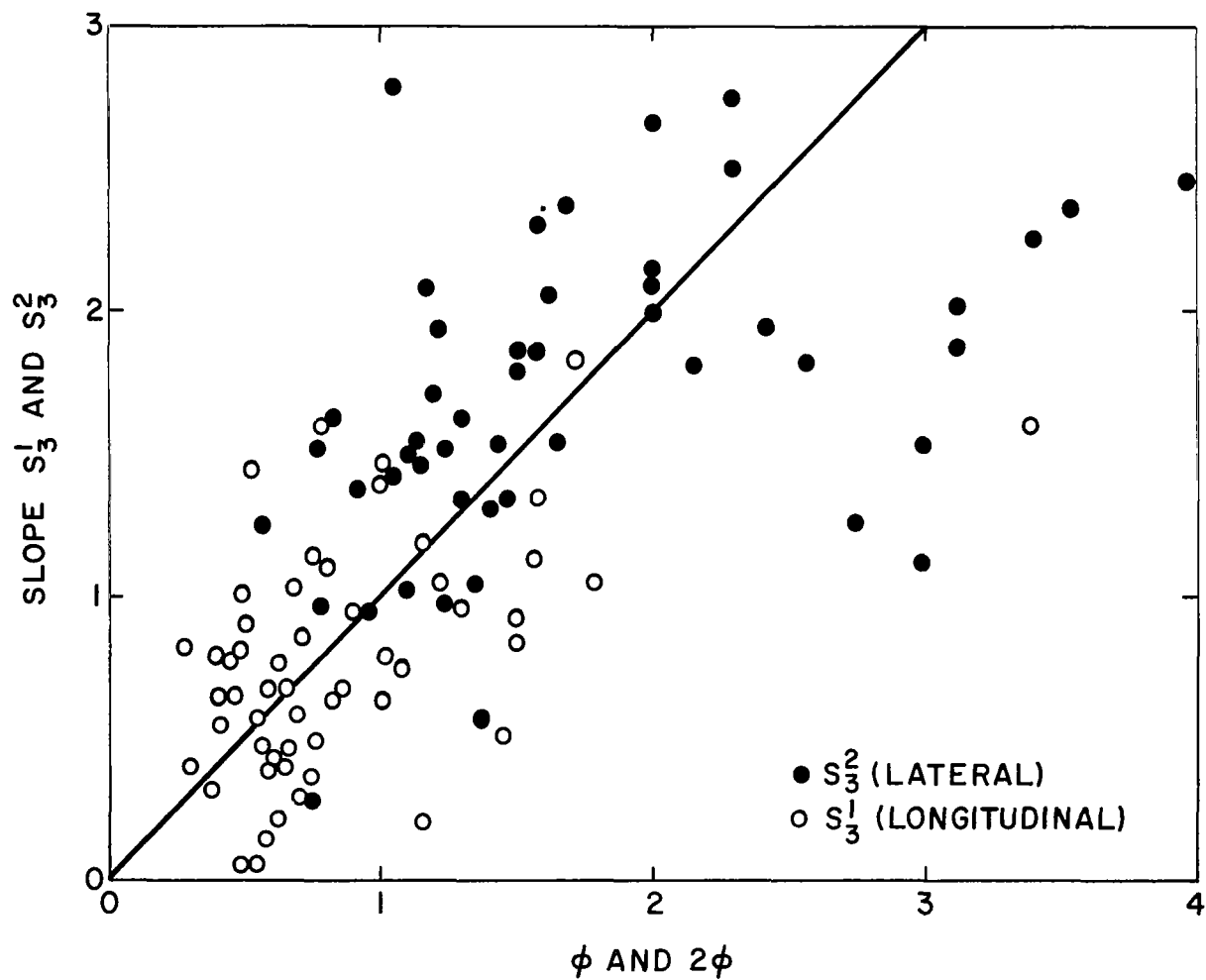


Figure 2.6 Slope of the longitudinal and lateral wind components between 18 m and 30 m as a function of the normalized wind shear.

2.4 Conclusions

The re-evaluation of Cape Kennedy data in conjunction with previous results strongly suggest constant values of $a_3^1 \sim 19$; $a_3^2 \sim 13$; $\text{slope}_3^1 \sim 1$ and $\text{slope}_3^2 \sim 2$ in neutral stratification below about 100 m.

The variation of slope with Richardson number Ri is proportional to the variation of ϕ . Also, the dependence of "a" is of a similar general character.

The decay constant at Kennedy in the vertical air are the same as those elsewhere in neutral air; but a discrepancy still exists in unstable air, where coherence at Kennedy is less than elsewhere.

REFERENCES

- Blackadar, A. K., J. A. Dutton, H. A. Panofsky, and A. Chaplin, 1969: Investigation of the turbulent wind field below 150 m altitude at the Eastern Test Range, NASA CR-1410, 92 pp.
- Businger, J. A., 1966: Transfer of momentum and heat in the planetary boundary layer. Proc. Symp. Arctic Heat Budget and Atmospheric Circulation, RM-5233-NSF, Rand Corp., 305 pp.
- Davenport, A. G., 1961: The spectrum of horizontal gustiness near the ground in high winds. Quart. J. R. Meteor. Soc., 87, 194-211.
- Marquardt, D. W., 1963: An algorithm for least-squares estimation of non-linear parameters. SIAM J. Appl. Math., 11, 431-441.
- McVehil, G. E., Jr., 1962: Wind distribution in the diabatic boundary layer. Unpublished Ph.D. Thesis, Dept. of Meteor., Pennsylvania State University.
- Monin, A. S., and A. M. Obukhov, 1954: Basic regularity in turbulent mixing in the surface layer of the atmosphere. Trudy Geophys. Inst. ANSSSR, 24, 163.
- Pandolfo, J. P., 1966: Wind and temperature profiles for constant flux boundary layers in lapse conditions with variable eddy conductivity to eddy viscosity ratio. J. Atmos. Sci., 23, No. 5, 495-502.

REFERENCES (continued)

- Pielke, R., 1969: Cross-spectral characteristics of temperature and longitudinal and lateral wind components. Unpublished Master's Thesis, Dept. of Meteor., Pennsylvania State University, 39 pp.
- Shiotani, M., 1969: Structure of gusts in high winds. Interim report, Physical Science Laboratories, Nihon University, Namashino, Japan, 60 pp.

III. THE ESTIMATION OF TOTAL DISSIPATION

R. C. Goff

3.1 Formulation of estimate

The total dissipation, E , is defined by

$$E = \int_{z_0}^{150} \rho \epsilon \, dz \quad (3.1)$$

where ρ is the density and ϵ the local dissipation. The lower limit z_0 follows from the convention that the ground is defined as $z = z_0$, where the wind speed vanishes.

An attempt was made to derive a method for estimating E from observations of temperature and wind at the lowest levels of the tower only, given the roughness length from a prior calibration of the site.

It was shown earlier (Blackadar, et al., 1969) that, above $z = 18$ meters, the dissipation was well described by:

$$\epsilon = \frac{u_{*0}^3}{kz} \left[\left(1 - 18 \frac{z}{L_0} \right)^{-1/4} - \frac{z}{L_0} \right] \quad (3.2)$$

where u_{*0} is the surface friction velocity and L_0 is the Lettau-Monin-Obukhov length obtained from observations near the ground.

Below $z = 18$ meters, the expression in brackets is small so that the fraction of E below 18 meters is

$$\frac{u_{*0}^3}{k} \ln \left(\frac{18}{z_0} \right)$$

Integration of Equation 3.2 from 18 meters to 150 meters shows that the fraction of E above 18 meters is given by:

$$E_T = \rho \frac{u_{*o}^3}{k} \left[\ln \frac{(1 - 18z/L_o)^{1/4} - 1}{(1 - 18z/L_o)^{1/4} + 1} \right] + 2 \tan^{-1} \left. \frac{(1 - 18z/L_o)^{1/4} - \frac{z}{L_o}}{1} \right|_{18}^{150} \quad (3.3)$$

z_o had been previously estimated as:

- a) 0.159 m for dense woods (Zone 1),
- b) 0.039 m for low scrub and sand (Zone 2),
- c) 0.121 m for low trees and hummocks (Zone 3).

The zones above are defined on the basis of the azimuth angle, θ , centered at the Kennedy tower, i.e.

- Zone 1 $180^\circ < \theta \leq 300^\circ$
- Zone 2 $300^\circ < \theta \leq 090^\circ$
- Zone 3 $090^\circ < \theta \leq 180^\circ$.

L_o was determined by first obtaining a Richardson number at 23 meters from the wind speeds and temperatures at 18 meters and 30 meters, and then putting $z/L_o \approx Ri$.

u_{*o} could then be obtained from:

$$u_{*o} = \frac{kV_{18}}{\ln \left(\frac{18}{z_o} \right) - \psi \left(z/L \right)} \quad (3.4)$$

3.2 Results

Table 3.1 gives the run numbers, L_o , and the "lower" ($z_o \leq z \leq 18$ m) and "upper" ($18 \leq z \leq 150$ m) portions of the estimated E, as well as the total E. Clearly, the contributions of these portions are of the same

TABLE 3.1

Vertically integrated dissipation of theoretical
and observed methods for various runs

Run	L_O	Lower E_T	Upper E_T	Total E_T	Lower E_O	Upper E_O	Total E_O
013	-575	9.27	2.64	11.90	11.08	1.43	12.52
030	-144	3.72	1.16	4.88	4.10	0.81	4.91
067	- 72	1.99	0.84	2.83	1.68	0.46	2.15
086	- 82	0.40	0.21	0.61	0.34	0.29	0.63
091	-136	1.51	0.62	2.13	2.64	1.33	3.96
133	-165	0.61	0.22	0.84	1.00	0.30	1.30
141	-10.0	0.24	0.53	0.77	0.56	0.45	1.01
149	-38.5	0.70	0.57	1.27	0.66	0.28	0.95
162	-115	0.47	0.21	0.68	0.68	0.18	0.86
163	- 70	0.33	0.17	0.50	0.50	0.54	1.04
165	-110	1.08	0.45	1.53	1.28	0.46	1.74
176	-21.4	0.15	0.20	0.35	0.22	0.15	0.37
182	- 50	0.60	0.33	0.93	0.98	0.48	1.45
183	- 59	0.33	0.16	0.48	0.70	0.76	1.46
189	-27.0	0.95	0.84	1.78	0.83	0.20	1.03
196	- 52	1.00	0.52	1.52	1.36	0.44	1.80
299	-344	1.81	0.65	2.46	1.49	0.85	2.35
305	-253	3.13	0.88	4.01	1.95	1.16	3.11
308	-377	8.88	3.20	12.01	4.33	1.25	5.58
309	-38.5	1.61	1.38	2.99	2.23	1.54	3.77
310	-140	8.55	3.48	12.03	10.70	4.21	14.92
316	-3.0	0.42	3.04	3.47	0.99	0.71	1.70
319	-9.1	0.57	1.38	1.94	0.98	1.41	2.39
326	- 71	0.60	0.31	0.91	0.77	0.90	1.67
335	- 66	0.48	0.21	0.70	0.82	0.65	1.47
337	- 55	4.11	2.08	6.18	3.44	1.79	5.23
351	-33.5	2.07	1.53	3.60	3.05	1.04	4.09
355	-39.2	0.30	0.19	0.49	0.47	0.64	1.12
359	-188	5.67	2.03	7.70	5.60	2.03	7.63

TABLE 3.1 (continued)

Run	L_o	Lower E_T	Upper E_T	Total E_T	Lower E_o	Upper E_o	Total E_o
361	-251	5.09	1.75	6.84	4.15	1.64	6.39
364	-484	1.15	0.64	1.78	1.16	0.62	1.78
365	-9.8	0.95	2.64	3.59	0.95	0.62	1.57
366	-46.5	1.17	0.67	1.84	1.58	1.27	2.85
406	-42.3	0.42	0.26	0.68	0.52	0.64	1.17
477	-20.0	1.23	0.43	1.66	1.95	0.60	2.55
515	-81	1.08	0.43	1.51	1.88	1.14	3.02
521	-316	2.12	0.72	2.84	3.80	1.24	5.04
526	-65	1.53	0.90	2.43	3.72	2.10	5.82
529	-284	1.10	0.31	1.40	1.44	0.68	2.12
551	-2.7	0.13	1.01	1.13	0.28	0.24	0.52
554	-14.1	0.28	0.45	0.73	0.34	0.31	0.65
554	-15.6	0.49	0.71	1.20	0.62	0.47	1.09
610	-16.9	0.52	0.86	1.37	0.64	0.39	1.03
618	-71	3.38	1.45	4.84	3.02	1.30	4.32

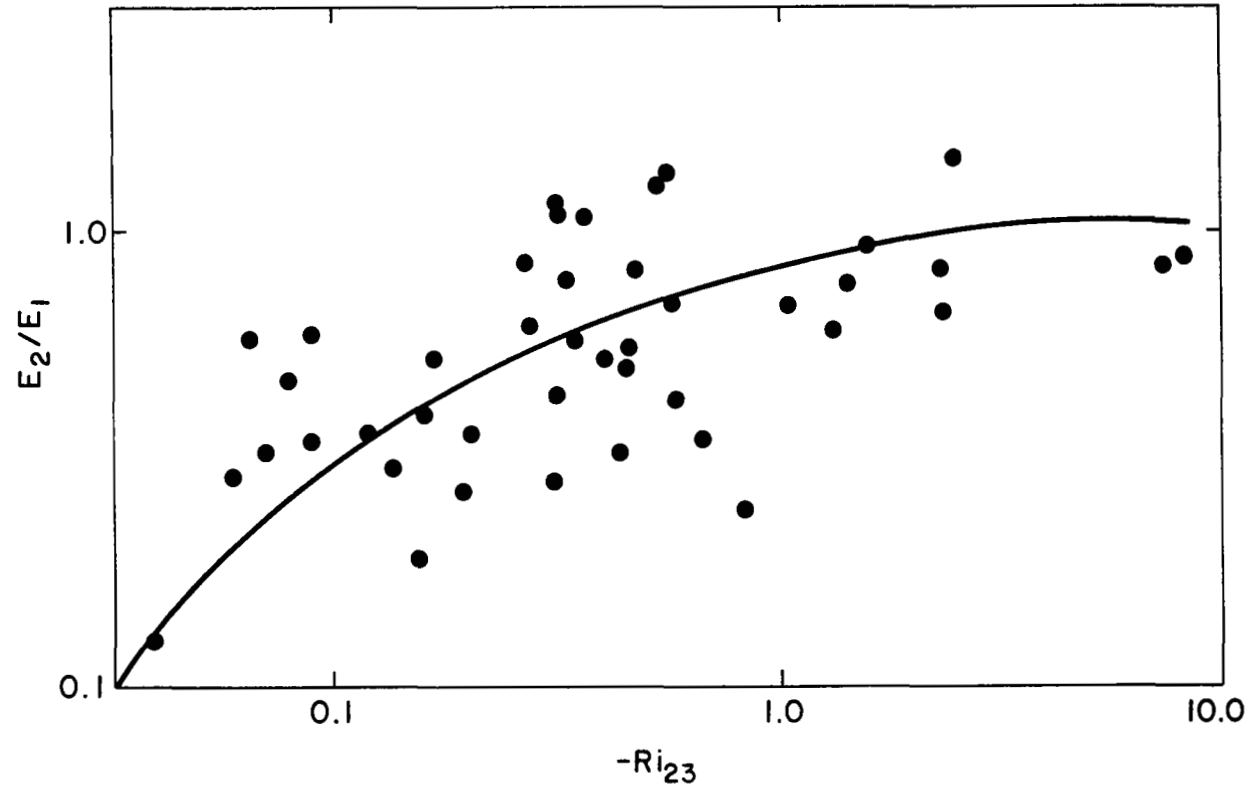


Figure 3.1 Ratio of the measured total dissipation above 18 m to the measured total dissipation below 18 m as a function of the gradient Richardson n-mber.

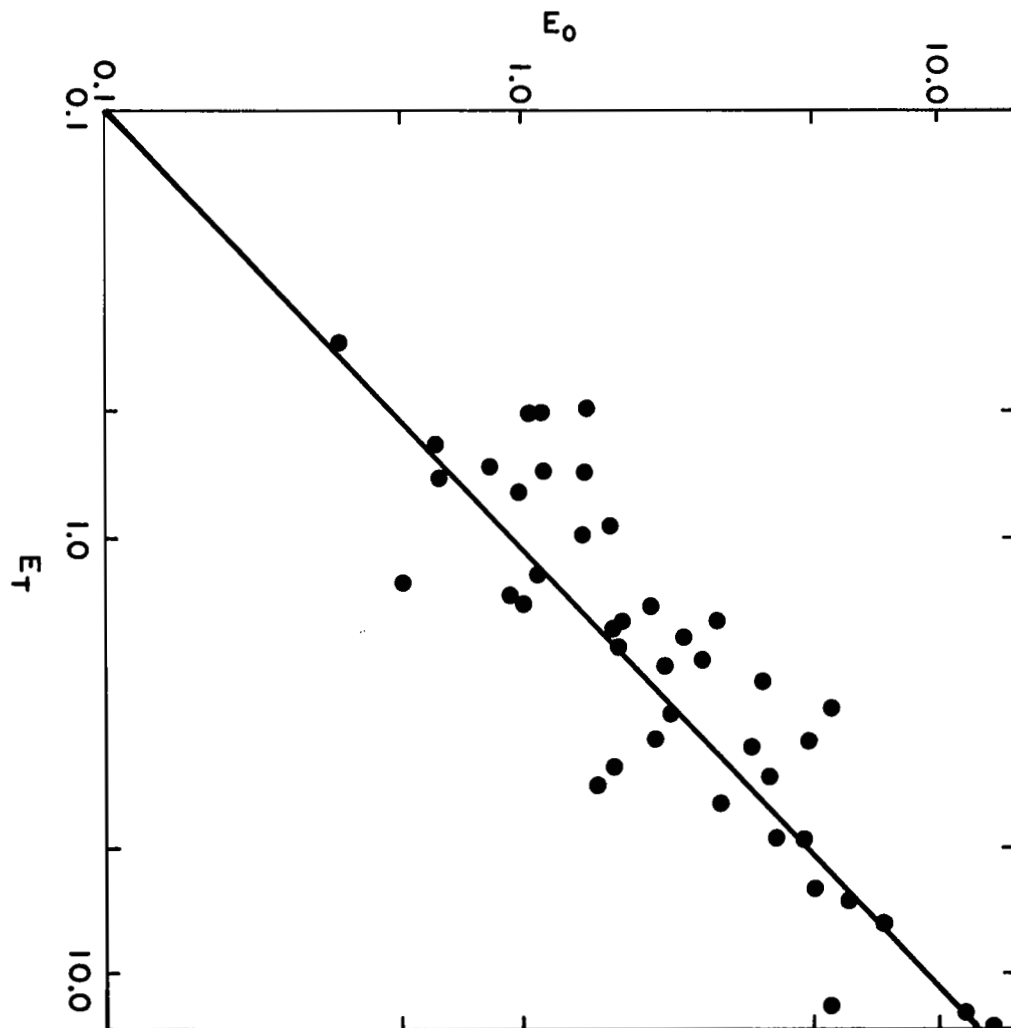


Figure 3.2 Comparison of the measured (E_a) and estimated (E_T) vertically integrated dissipation in watts/m² at and below 18 m.

order of magnitude; the upper portions are relatively larger, the more unstable the air (see Fig. 3.1).

The estimates of E were compared with "observed" E. Below 18 meters, the same formula was used as that for the estimated values, except that "observed" z_0 values were used for each run. At and above 18 meters, values of local dissipation were computed from the high frequency portion of the spectra of the longitudinal wind component

$$\epsilon = \left[S(k)/b \right]^{3/2} k_1^{5/2} \quad (3.5)$$

where $b = 0.14$ for longitudinal spectra and 0.18 for lateral spectra and k_1 is the wave number in radians per unit length. The integral in Equation 4.1 was evaluated by the trapezoidal approximation between 18 and 150 meters from observations at six levels.

Table 3.1 also lists observed lower and upper portions of E, as well as total E, and Figure 3.2 compares "observed" and "estimated" total E. There is a fair amount of scatter in the figure, but no systematic difference between ordinate and abscissa.

REFERENCES

- Blackadar, A. K., J. A. Dutton, H. A. Panofsky, and A. Chaplin, 1969:
Investigation of the turbulent wind field below 150 m altitude at
the Eastern Test Range, NASA CR-1410, 92 pp.

IV. ESTIMATION OF VARIANCES

H. A. Panofsky and V. Mirabella

4.1 Variances at 18 meters

According to Monin-Obukhov similarity theory, the standard deviations of longitudinal and lateral wind components are given by:

$$\sigma_u = \phi_u (z/L) u_* \quad (4.1)$$

$$\sigma_v = \phi_v (z/L) u_* \quad (4.2)$$

Here u_* is the friction velocity and ϕ_u and ϕ_v are universal functions of z/L where L is the Lettau-Monin-Obukhov length. Whereas it is generally agreed that expressions of the form of Equations 4.1 and 4.2 fit statistics of the vertical velocity quite well, there is considerable doubt about the adequacy of the equations for σ_u and σ_v . Nevertheless, these equations will be used in an attempt to understand these variables.

First, u_* was estimated from the wind equation:

$$u_* = \frac{k\bar{V}}{\ln z/z_o - \psi(Ri)} \quad (4.3)$$

where \bar{V} is the mean wind at a low level (here taken to be 18 m), z_o is the roughness length, $\psi(Ri)$ is a universal function well known in unstable air and k is the von Karman's constant which is usually taken as 0.4.

Ri was estimated from the temperatures and wind at 18 m and 30 m (so that it applies at 23 m), and then multiplied by 18/23 to yield a value at 18 meters according to Businger's hypothesis. The roughness lengths used were those computed from observed spectra at high frequencies, as suggested by Panofsky (1969).

Figures 4.1 and 4.2 show the relations between the standard deviations and the friction velocity at 18 meters. Straight lines with slopes of 2.3 fit the data reasonably well, with standard deviations of .19 and .29 for the longitudinal and lateral velocity components, respectively. These lines were fitted by least squares and forced to pass through the origin. As can be seen from the graphs, the scatter is greater for the lateral component than the longitudinal component. This can be partially explained by the fact that the ratio σ_u/u_* is relatively insensitive to changes in stability as is shown in Figures 4.3 and 4.4.

In the estimates of variance described so far, it was assumed that separate roughness lengths could be obtained for each run from observed spectra at all tower levels. In many practical situations, the site will have been "calibrated" previously so that roughnesses can be preassigned, often varying with wind direction. In the case of the Kennedy tower, the values of z_o adapted on the basis of prior work are given in the article by Panofsky (1969) and since slightly modified. Revised friction velocities were calculated based on these roughness lengths.

Figures 4.5 and 4.6 show σ_u and σ_v as functions of these estimates of u_* . The slope in the case of σ_u is about 2.24 and the scatter is slightly less than in Figure 4.1. This suggests that the average values of z_o in the various sectors are more nearly correct (less influenced by random error) than the z_o 's observed separately for every run. Figure 4.5 itself leads to a good estimate of σ_u at 18 meters given u_* from Equation 4.3. The slope for σ_v is about 2.27 and the scatter is also slightly less than that of Figure 4.2.

Figures 4.7 and 4.8 show the variations of $(\sigma_u/u_*)_{18}$ and $(\sigma_v/u_*)_{18}$ as a function of the Richardson Number at 18 meters using the zone z_o 's. The

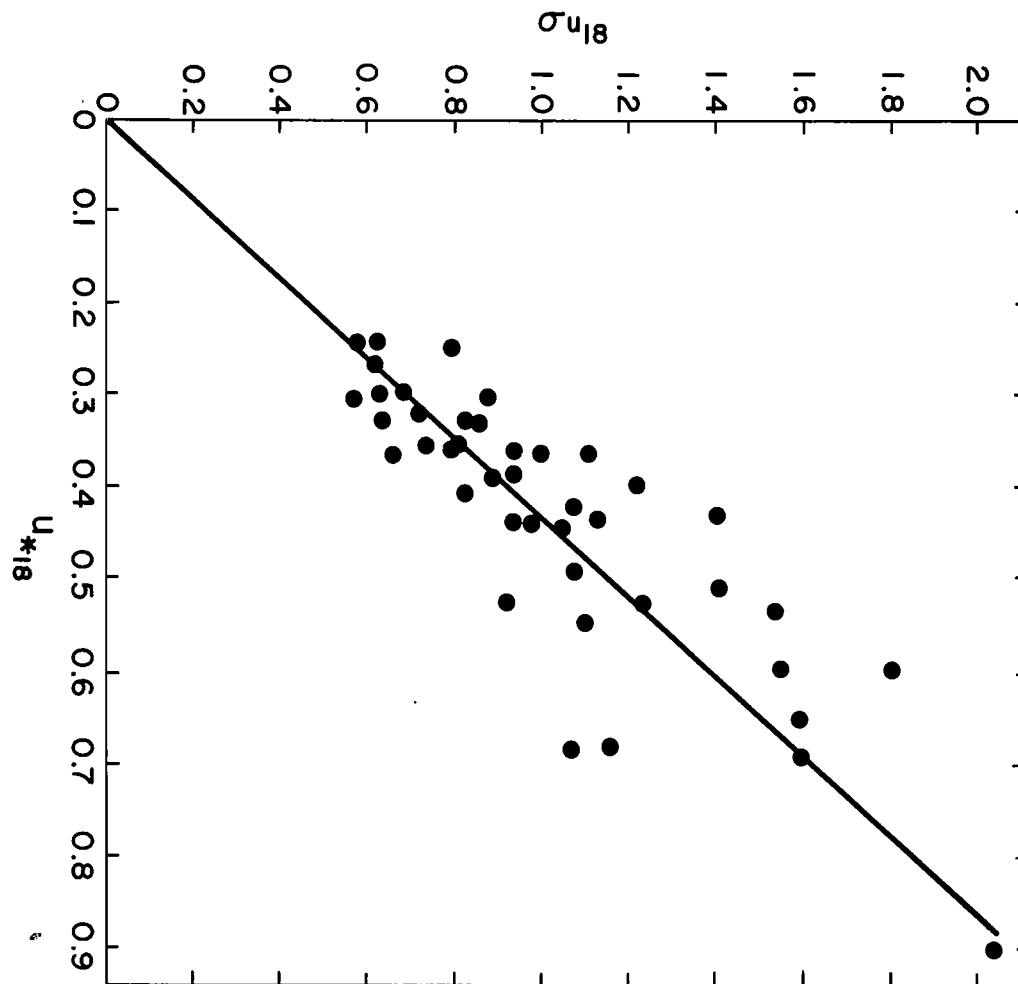


Figure 4.1 Variance of the longitudinal wind components at 18 m as function of friction velocity at 18 m utilizing a roughness length determined for each run separately.

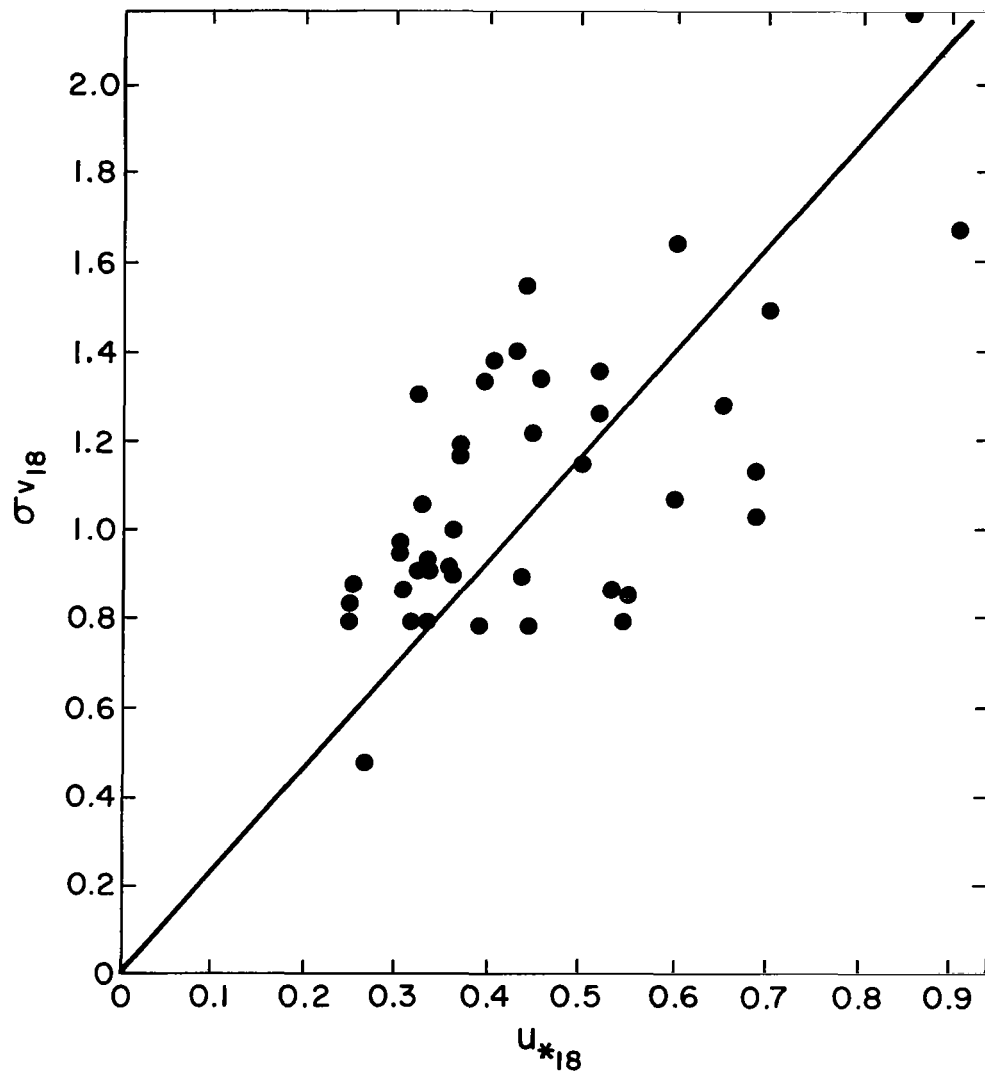


Figure 4.2 Variance of the lateral wind components at 18 m as a function of friction velocity at 18 m utilizing a roughness length determined for each run separately.

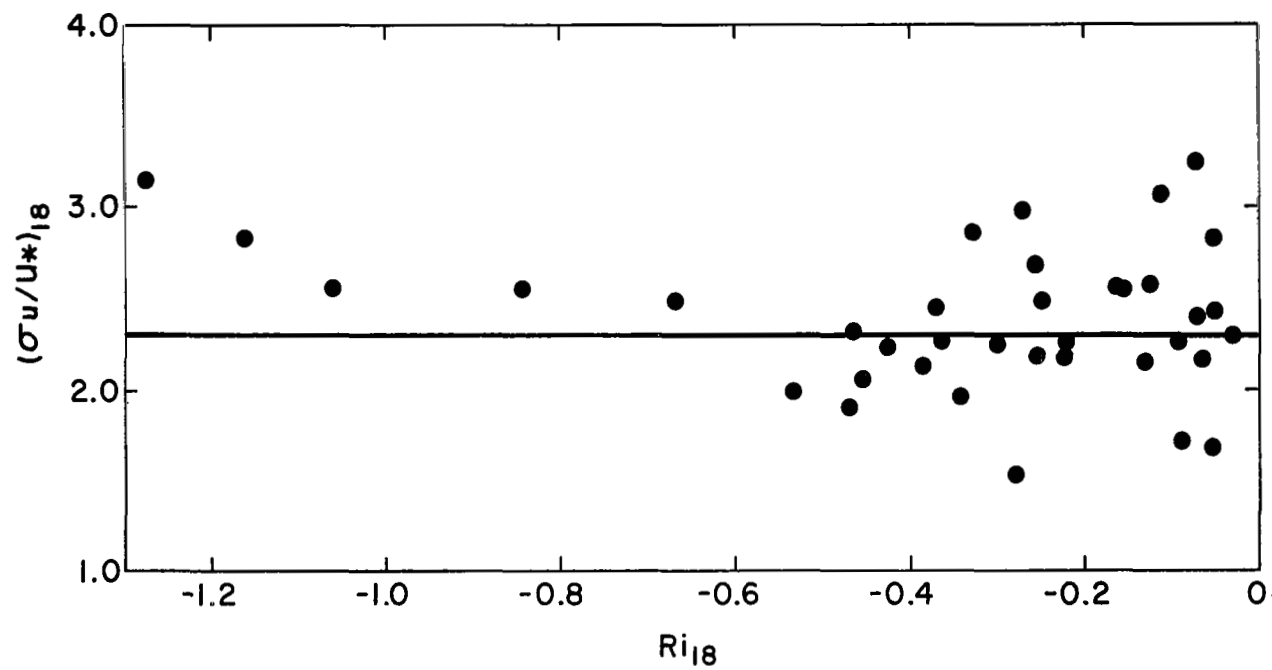


Figure 4.3 Ratio of the variance of longitudinal wind components to friction velocity at 18 m as a function of the Richardson number at 18 m utilizing a roughness length determined for each run separately.

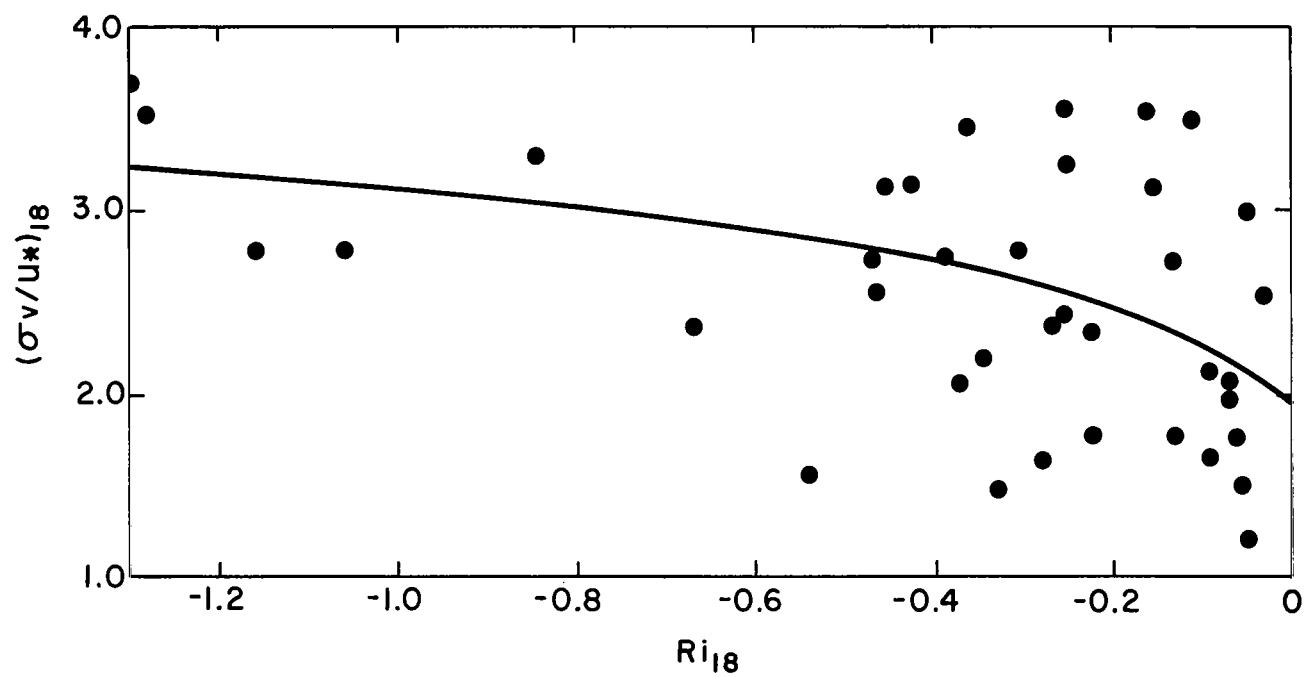


Figure 4.4 Ratio of the variance of lateral wind components to friction velocity at 18 m as a function of the Richardson number at 18 m utilizing a roughness length determined for each run separately.

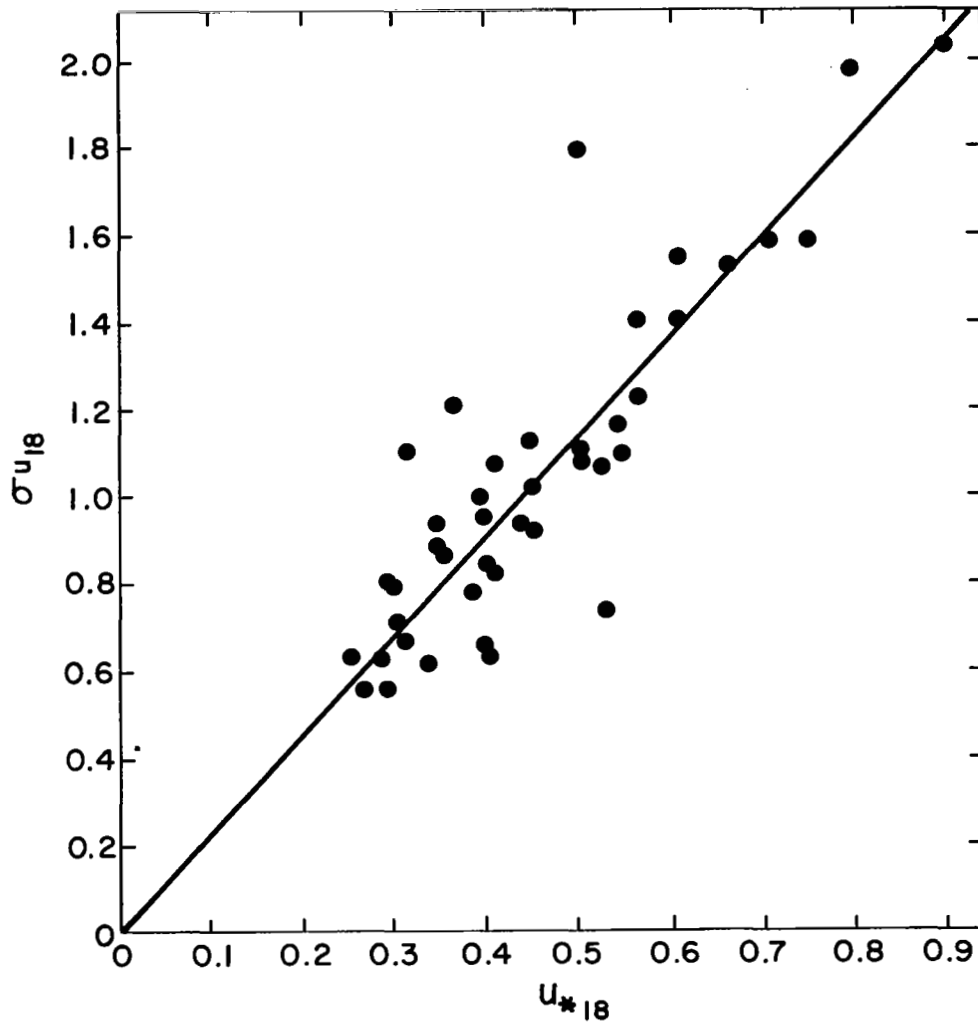


Figure 4.5 Variance of the longitudinal wind components at 18 m as a function of friction velocity at 18 m utilizing a roughness length determined from average upwind zone conditions.

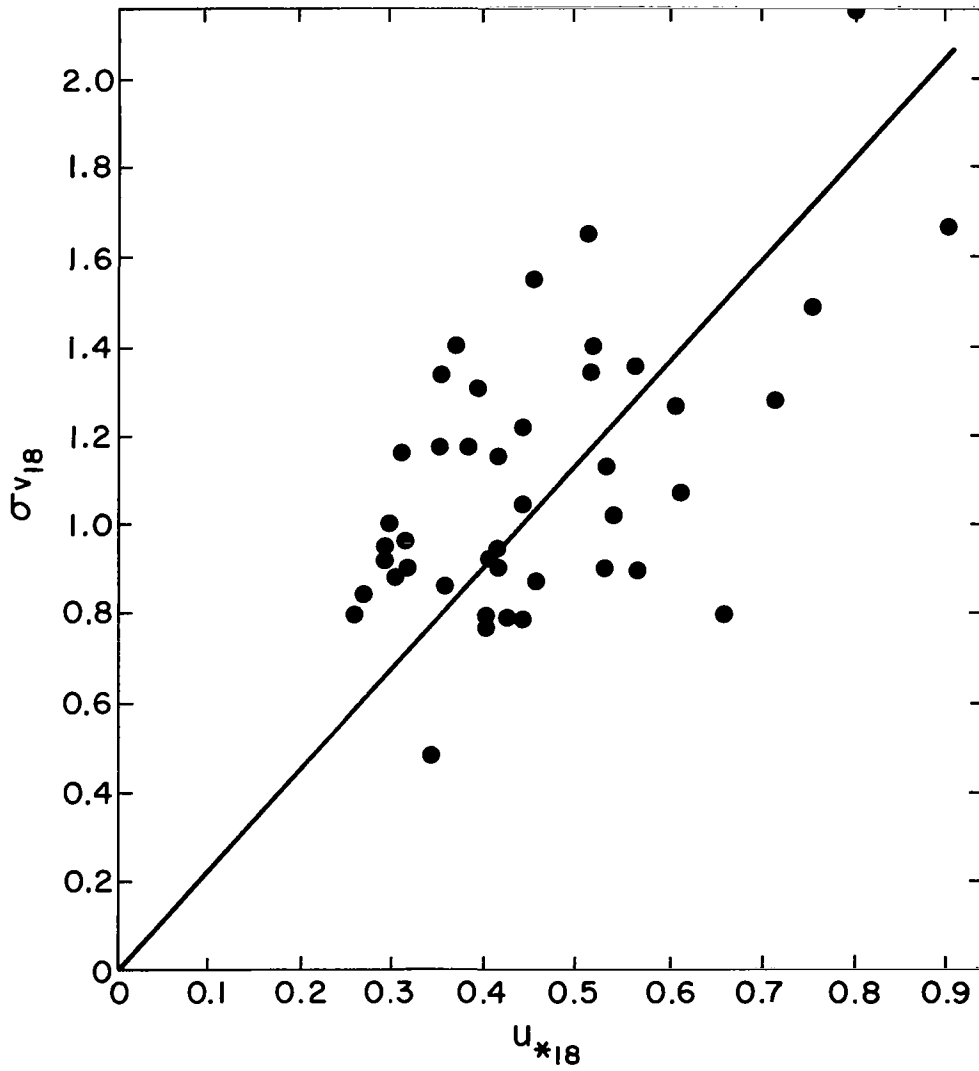


Figure 4.6 Variance of the lateral wind components at 18 m as a function of friction velocity at 18 m utilizing a roughness length determined from averaged upwind zone conditions.

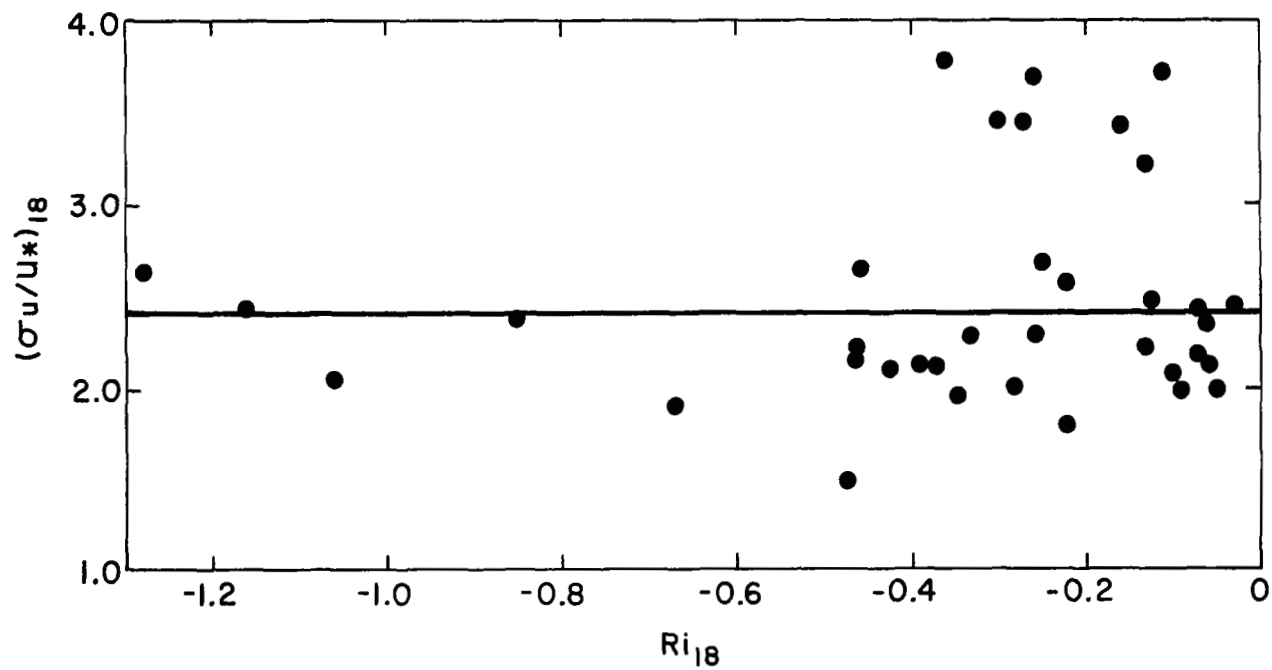


Figure 4.7 Ratio of the variance of longitudinal wind components to the friction velocity at 18 m as a function of the Richardson number at 18 m utilizing a roughness length determined from averaged upwind zone conditions.

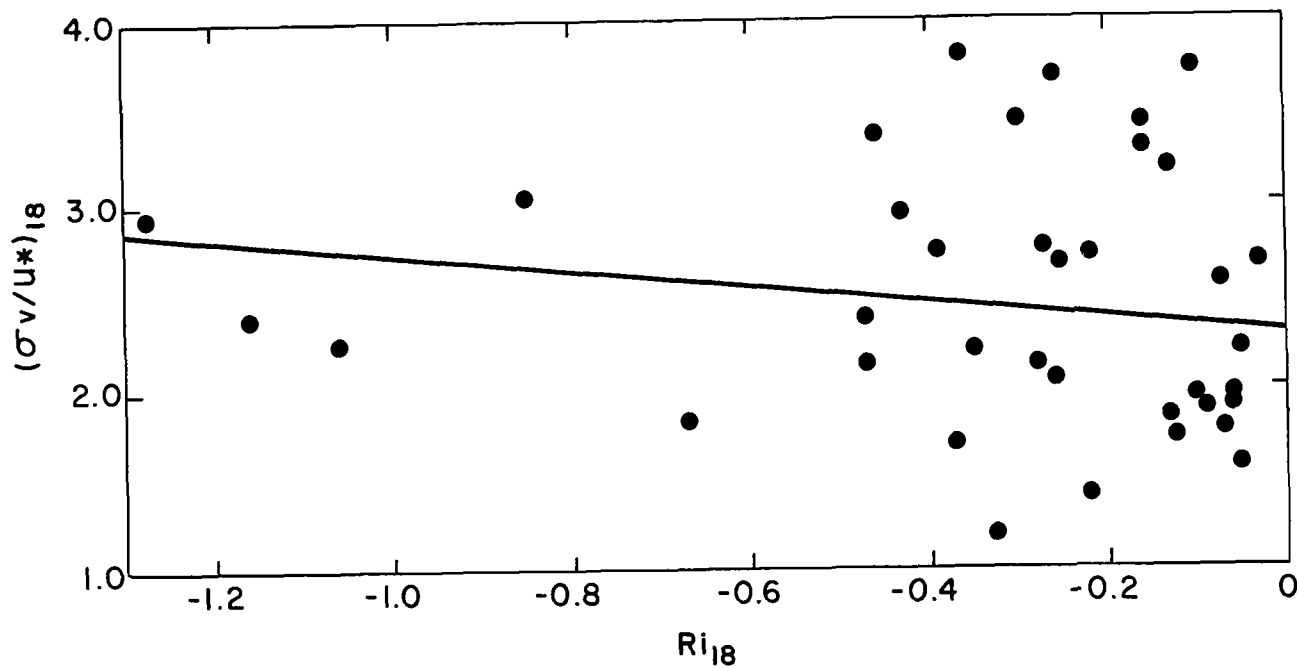


Figure 4.8 Ratio of the variance of the lateral wind components to the friction velocity at 18 m as a function of the Richardson number at 18 m utilizing a roughness length determined from averaged upwind zone conditions.

scatter of the points about the line for σ_u/u_* in Figure 4.7 is essentially independent of Richardson Number, showing that σ_u can be taken as a constant at 18 meters within the experimental error. As was the case for Figure 4.4, the ratio σ_v/u_* as computed with the sector z_0 's is correlated with Ri as shown in Figure 4.8. This type of relation would also be expected from Prasad's summary (1967). In other words ϕ_v varies with Ri from about 2.3 in neutral air to about 3.0 in very unstable air.

Presumably, optimum estimates of σ_v at 18 meters would be obtained by computing u_* from Equation 4.3 and then multiplying by σ_v/u_* given by Figure 4.8. Still the statistical error would be large.

4.2 Change of variances with height

Let

$$\sigma_{u_{150}} = \phi_{150} u_{*_{150}} \quad (4.4)$$

and

$$\sigma_{u_{18}} = \phi_{18} u_{*_{18}} \quad (4.5)$$

where ϕ_{150} and ϕ_{18} are constants, and the subscripts refer to height in meters.

Subtracting Equation 4.4 from Equation 4.5, we find

$$\sigma_{u_{18}} - \sigma_{u_{150}} = (\phi_{18} - \phi_{150}) u_{*_{18}} + \phi_{150} \beta (150 - 18) \quad (4.6)$$

where $\beta = - \frac{\partial u_*}{\partial z}$.

Given an estimate of $\sigma_{u_{18}}$ from Figure 4.5 we can estimate $\sigma_{u_{150}}$ from Equation 4.6 if we know its right hand side. The quantity β follows from the equations of motion (neglecting accelerations)

$$\beta = \frac{f}{2} \frac{V_g}{u_*} \quad (4.7)$$

Here, f is the Coriolis parameter and V_g the component of the geostrophic wind at right angles to the surface wind. The ratio V_g/u_* is theoretically a constant in neutral air and has been recently been found to be the same constant in unstable air as well (Sheppard, to be published, 1970). Thus, the last term in Equation 4.6 can be taken as constant at a given latitude in neutral and unstable air.

If $\phi_{18} = \phi_{150}$, $\sigma_{u_{18}} - \sigma_{u_{150}}$ should be independent of wind speed. To test this hypothesis, Figure 4.9 gives the relation between $\sigma_{u_{18}} - \sigma_{u_{150}}$ and the wind at 18 meters. Apparently, there is quite a strong relationship. Hence $\phi_{18} = \phi_{150}$. However, Figure 4.9 can be used to estimate $\sigma_{u_{18}} - \sigma_{u_{150}}$ given \bar{V}_{18} . Once this difference is given, σ_u at other levels can also be determined since the distribution of σ_u with height is approximately linear.

Actually, there is reason to doubt that the relation between u_* and σ_u should be different at different levels. If the relation is general, the observations here could be explained if the values of σ_u at 150 m had been underestimated by perhaps 10%, possibly because low frequencies which had been filtered out in the analysis procedure, contributed more to $\sigma_{u_{150}}$ than to $\sigma_{u_{18}}$.

An analogous procedure is performed for the change of σ_v with height and Figure 4.10 is a plot of $\sigma_{v_{18}} - \sigma_{v_{150}}$ as a function of the wind at 18 meters. The scatter is quite large probably due to the fact that the terms depend upon stability.

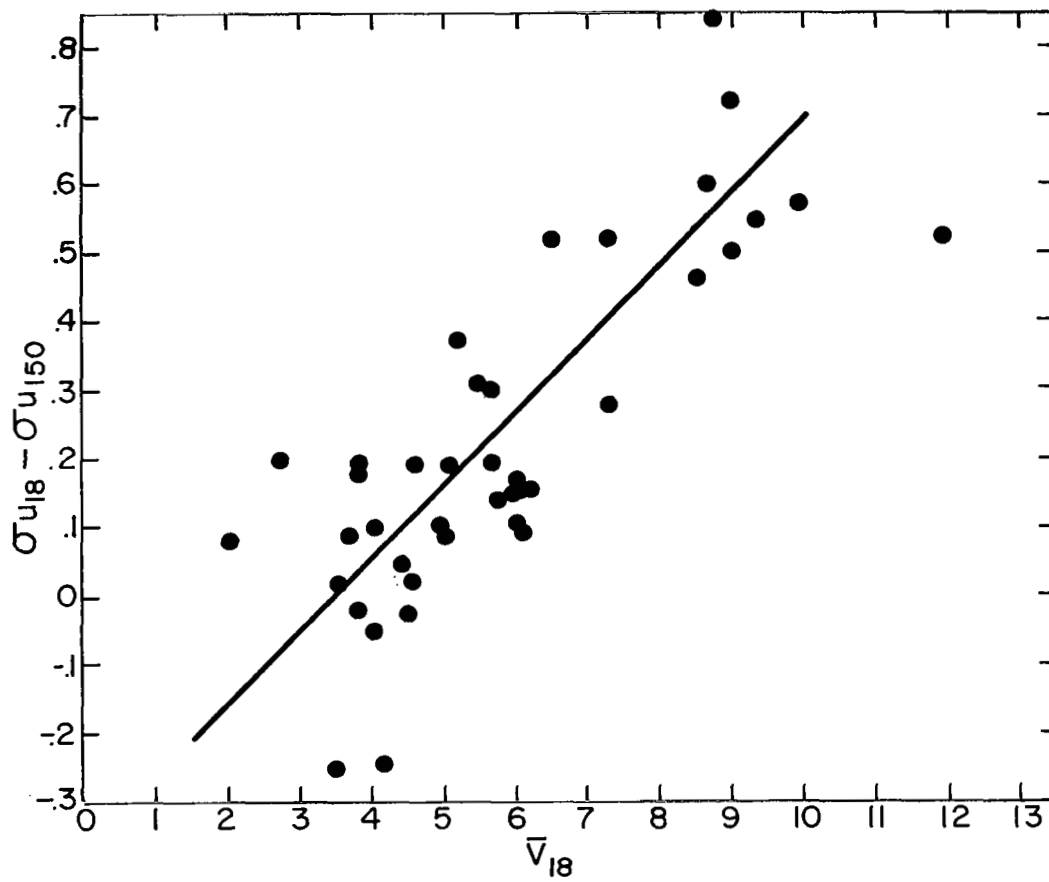


Figure 4.9 Difference of the variances of the longitudinal wind component at 18 m and 150 m as a function of the mean wind at 18 m.

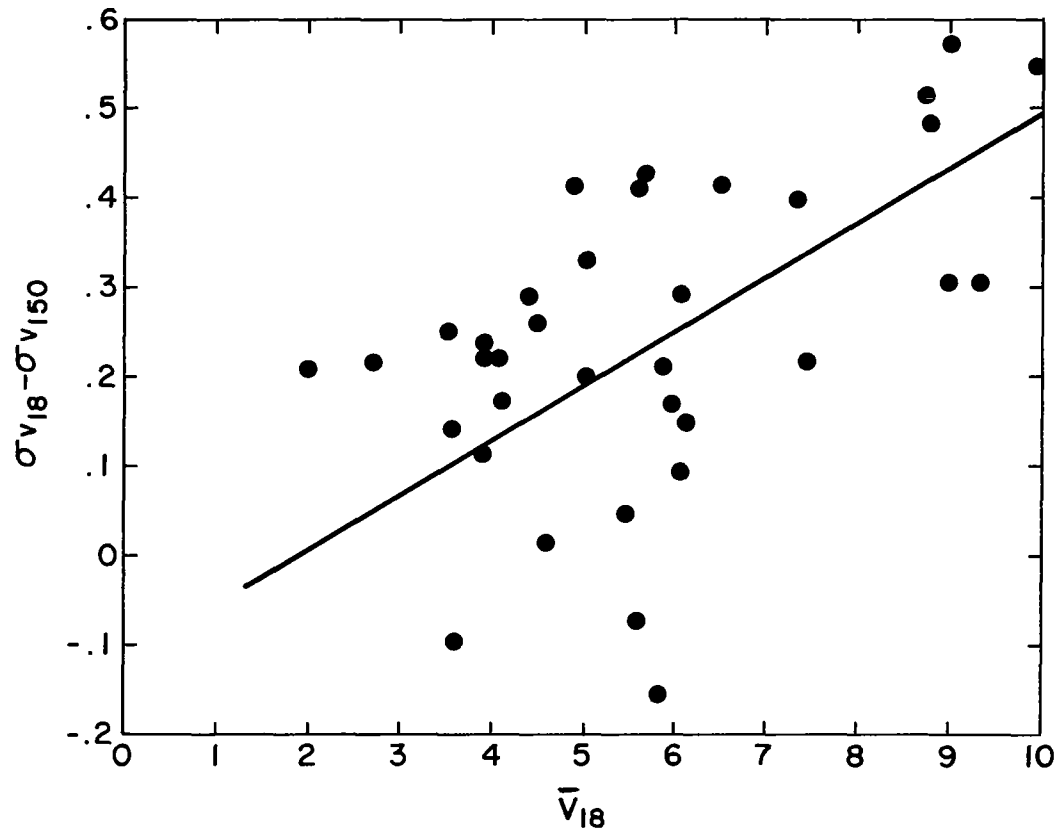


Figure 4.10 Difference of the variances of the lateral wind component at 18 m and 150 m as a function of the mean wind at 18 m.

REFERENCES

- Panofsky, H. A., 1969: Spectra of the horizontal wind components in "Investigation of the turbulent wind field below 150 m altitude at the Eastern Test Range", (Blackadar, A. K. et al.), NASA CR-1410, 92 pp.
- Panofsky, H. A., and B. A. Prasad, 1965: Similarity theories and diffusion, Air and Water Pollution, 9, 419-430.
- Prasad, B. A., 1967: Wind and temperature fluctuation in the surface layer. Ph.D. Thesis, Pennsylvania State University, Dept. of Meteorology, 77 pp.
- Sheppard, P. A., 1970: To be published.

MSFC-RSA, Ala